

# IMPERIAL

*Spirals, defects, rolls and bands;*  
**Transitional Rayleigh-Bénard Poiseuille flows  
using spectral/*hp* element methods**

---

*BY*

**Chi Hin Chan**

*SUPERVISED BY*

Professor Spencer J. Sherwin  
&  
Professor Yongyun Hwang

*at the*

DEPARTMENT OF AERONAUTICS  
FACULTY OF ENGINEERING  
IMPERIAL COLLEGE LONDON

THIS THESIS IS SUBMITTED FOR THE DEGREE OF DOCTOR OF PHILOSOPHY



# **Declarations**

## **Statement Of Originality**

I certify that the content of this thesis is a product of my own work. I have appropriately acknowledged any other material that may have been used through standard referencing practices.

## **Copyright Declaration**

The copyright of this thesis rests with the author. Unless otherwise indicated, its contents are licensed under a Creative Commons Attribution-Non Commercial 4.0 International Licence (CC BY-NC). Under this licence, you may copy and redistribute the material in any medium or format. You may also create and distribute modified versions of the work. This is on the condition that: you credit the author and do not use it, or any derivative works, for a commercial purpose. When reusing or sharing this work, ensure you make the licence terms clear to others by naming the licence and linking to the licence text. Where a work has been adapted, you should indicate that the work has been changed and describe those changes. Please seek permission from the copyright holder for uses of this work that are not included in this licence or permitted under UK Copyright Law.



# Abstract

The transitional regimes of Rayleigh-Bénard Poiseuille (RBP) flows and Rayleigh-Bénard convection (RBC) are investigated using direct numerical simulations and linear stability analysis. RBP flows serve as a paradigmatic configuration that describes fluid motion driven by shear and buoyancy forces, a combination of the classical buoyancy-driven RBC and shear-driven plane Poiseuille flow (PPF). While the transitional regime of RBC and PPF have been well studied over the past century, the transitional regime where both forces interact remains largely unexplored beyond linear instability.

Following a review of the relevant literature and numerical methods, we conduct direct numerical simulations of transitional RBP flows using Nektar++, a spectral/ $hp$  element package. The simulations span over a range of Rayleigh numbers,  $Ra \in [0, 10000]$  and Reynolds number  $Re \in [0, 2000]$ , with unit Prandtl number in a large computational domain. Within this parametric space, we identify five distinct regimes: (1) bistable SDC & ISRs, (2) ISRs, (3) wavy rolls, (4) intermittent rolls, and (5) shear-driven turbulence. The (4) intermittent rolls regime represent a newly identified state characterised by the spatio-temporal intermittent breakdown and regeneration of longitudinal rolls. In the (5) shear-driven turbulent regime, we also observe that intermittent rolls may coexist with turbulent-laminar bands. The spatio-temporal intermittent dynamics of longitudinal rolls highlight its dominant role in transitional RBP flows. To suppress spatial intermittency, we examine the unstable manifolds of the longitudinal rolls in a confined domain, integrating along which leads to turbulence. Depending on  $Re$ , this turbulence may occur transiently, decaying towards the unstable laminar base state where the longitudinal rolls can be excited again, forming a quasi-cyclic process referred to as the *thermally-assisted sustaining process (TASP)*. We furnish a state space sketch of the dynamical process, and discuss the relevance of the *TASP* to larger domains, concluding the first part of the thesis.

In the second part, we explore the state space structure of the bistable system between spiral defect chaos (SDC) and ideal straight rolls (ISRs) of Rayleigh-Bénard convection within large domains. By systematically reducing the domain size, we observe that SDC occurs transiently, eventually stabilising into multiple stable invariant solutions, referred to as *elementary states*. These *elementary states* are visually and statistically similar to the localised features of SDC, underpinning the pattern formation of SDC. We also examined the edge between the basin of attractions of ISRs and the elementary states, revealing multiple edge states. Investigating the unstable manifolds of ISRs exhibit two distinct behaviours: (1) unstable ISRs near the Busse balloon connect to stable ISRs and base state via heteroclinic connections, and (2) unstable ISRs further from the Busse balloon lead to SDC, indicating such ISRs lie on boundary between ISRs and SDC. Finally, we present a state space sketch of the *elementary states* organised around SDC, highlighting its ‘building-block’ description of SDC.



# Acknowledgements

There are many people who have shaped my experience as a PhD student whom I would like to express my gratitude for. First and foremost, I want to express my deepest gratitude to my supervisors, Spencer and Yongyun. I have learned and grown a lot under their tremendously kind and patient supervision. It is a truly a pleasure to learn from world leading experts in fluid mechanics and computational fluid dynamics, and I will miss the knowledge osmosis process during our weekly catch-ups. Apart from the PhD, they also openly supported personal development opportunities, allowing me to pursue interests such as the Nektar++ redesign project, engaging in graduate teaching assistant roles, pursuing a summer research exchange at LadHyX and an internship at IBM Research, which I am grateful for.

I would like to specially thank Yongyun, who also happens to be my MSc thesis supervisor. Together, we worked the topic of reduced-order modelling of turbulent Couette flows as part of my MSc thesis. Perhaps more importantly, for giving me the confidence I needed to pursue a PhD program at Imperial.

I would also like to thank Lutz, for his kind hospitality, ensuring that I was comfortable at LadHyX in the summer of 2024. Despite being a short three months stint, I learned about advanced modal decomposition techniques and was exposed to the broad fluid mechanics research activities at LadHyX.

I would also like to thank Basman, my Bachelor's thesis supervisor at Nanyang Technological University (NTU), during which we worked on humpback whale leading-edge tubercles for my FYP. I believe it is fair to say that he was primarily responsible for planting the "seed" for my fascination for computational fluid dynamics.

I would also like to thank the Nektar++ community, particularly Henrik, Alex, Chris, Jacques and Dave for their timely responses on compilation errors, segmentation faults and guidance on software principles for contributing to Nektar++.

I would also like to thank my collaborators, Mohammad and Raj, for providing invaluable guidance and advice during the PhD, and also the opportunity to collaborate on physics-informed neural networks.

I would like to also thank Eloisa and Geeth, my project supervisor and manager at IBM Research, for giving an eye-opening opportunity to learn and contribute to AI research activities in a corporate company.

I would thank my fellow PhD students and postdocs from the office, for their endearing support over the 'instabilities' of PhD and London life. I will fondly remember our shared experiences such as unwinding over a cheeky pint on Friday evenings, mario karting in the common room, going to Sagar and exploiting its 50% discount, honest burgers student discounts, going to Wasabi at South

---

Kensington at closing to get half-priced bentos, countless muffin (Toffee banana is the best) and coffee breaks, peaceful walks around campus, Hyde park runs, booking the swimming pool sessions just to use the sauna, many gym/swim/badminton/climbing sessions, appearing decently surprise to bump into each other in the office on the weekends, and bantering over the weather, reviewers and PhD life. Special thanks to Henrik, Parv, Alex, Kaloyan, Ganlin, Steffi, Lidia, Christian, Kazuki, Priyam, Sid, Elise, Yu Hang, Cheng Wei, Zhao, Zilin, Victor, Mohsen, Guglielmo, João, Yacine and many others, all of whom made London feel like home.

The person who probably deserves the most credit would be my fiancée, Angelica, who have been there at the beginning, ready to lend a listening ear to my monologue on how cool CFD is. The distance between Singapore and London has been tough over the years, and I look forward to building our shared future after the PhD. Last but not least, I am grateful to my loving parents and family, for supporting my academic interests and developments aboard despite the distance.

I would like to acknowledge the generous financial support from the Imperial College President's PhD scholarships, Global Fellows Fund and computing resources from ARCHER2, without which this PhD would not have been possible.

Chi Hin Chan  
London  
November 2025

# Contents

<b>1</b>	<b>Introduction</b>	<b>1</b>
1.1	Overview . . . . .	1
1.2	Transitional wall-bounded shear flows . . . . .	4
1.2.1	Linear Stability Analysis . . . . .	4
1.2.2	Nonlinear dynamical systems . . . . .	8
1.2.3	Self-sustaining process . . . . .	11
1.2.4	Spatiotemporal transitional flows . . . . .	12
1.3	Rayleigh-Bénard convection . . . . .	15
1.4	Rayleigh-Bénard Poiseuille (RBP) flows . . . . .	20
1.5	Thesis Outline . . . . .	22
<b>A</b>	<b>Appendices</b>	<b>25</b>
A.1	Simulation parameters for $Ra$ - $Re$ sweep . . . . .	25
A.2	1st and 2nd order statistics . . . . .	25
A.2.1	Buoyancy-driven regime . . . . .	25
A.2.2	Shear-driven regime . . . . .	28
A.3	Growth rates of primary instabilities . . . . .	28
A.4	Verification of linear stability analysis . . . . .	32
A.5	Other elementary states and ISRs . . . . .	32



# Chapter 1

## Introduction

### 1.1 Overview

Fluid motions driven by buoyancy and frictional forces belongs to class of flows known as thermoconvective shear flows. These flows exhibit rich behaviour, and are of interest in both engineering and meteorology applications spanning across a broad range of length scales.

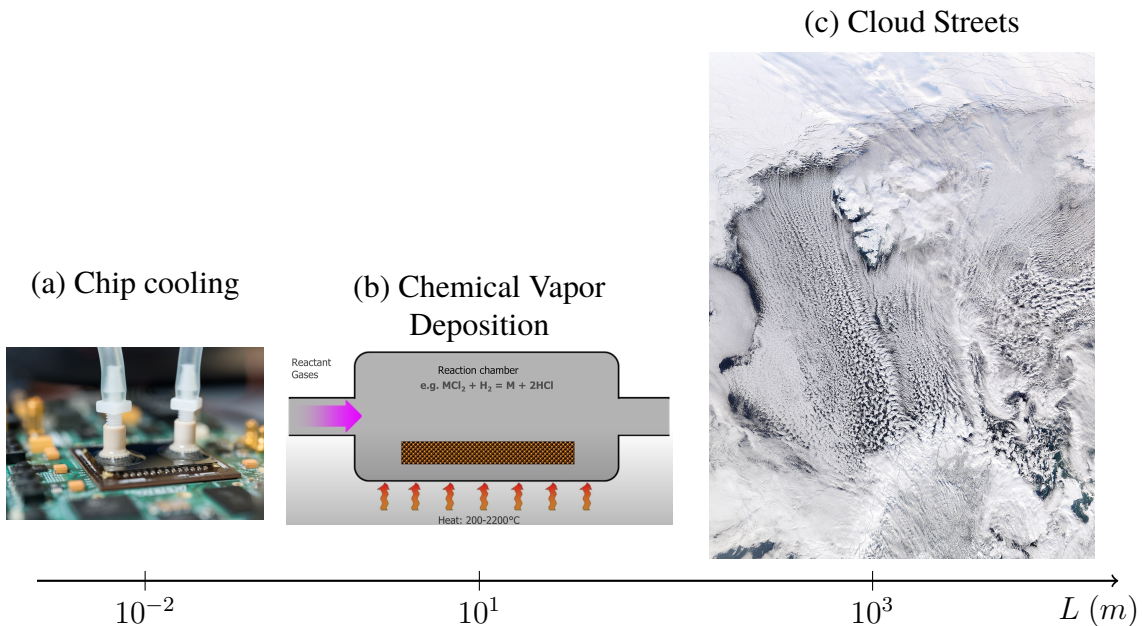


Figure 1.1: Thermoconvective shear flows driven by shear and buoyancy forces across length scales,  $L \in [10^{-2} m, 10^3 m]$ . Examples include (a) chip cooling, (b) chemical vapour deposition and (c) the formation of cloud streets.

At small scales, around  $L \sim 10^{-2} m$ , thermoconvective flows are relevant to the cooling of microprocessing chips. The fluid, acting as a medium for dissipating heat, experiences shear and buoyancy forces from the confining walls, and heating. One of the major challenge in this industry is on increasing the density of transistors on a single chip, alluding to Moore's Law, predicting the doubling of transistors on a single chip approximately every two years. One of the major limitations is the challenge of dissipating the excessive heat generated from the densely packed transistors. Fluids,

such as air, water or refrigerants, are often used to transport heat away from the components, and their transport behaviour under the influence of buoyancy and shear remains an open topic ([Kennedy & Zebib, 1983](#); [Ray & Srinivasan, 1992](#)).

At intermediate length scales,  $L \sim 1m$ , the interaction between buoyancy and frictional forces is important in the fabrication of uniform thin films in chemical vapour deposition (CVD) ([Evans & Greif, 1991](#); [Jensen, Einset, & Fotiadis, 1991](#)). The CVD process typically involves a reactive gases carried by inert gases which flows through a channel with a heated substrate. Upon heating, the reactant gases react chemically on the substrate, depositing material and forming thin films, such as silicon layers. A key challenge in the CVD process is achieving a uniform deposition and maintaining sharp interfaces between layers. The interactions between shear and buoyancy forces often gives rise to boundary layers and thermoconvective rolls, which can disrupt uniform deposition, affecting film quality.

At larger length scales,  $L \sim 10^3 m$ , the thermoconvective shear flows can be observed in atmospheric flows such as the cloud streets over the Norwegian Sea. These parallel bands of cumulus clouds can stretch over hundreds of kilometres. They form when the relatively warmer sea surface heat up the colder air arriving from the North pole. As the colder air is heated, it rises upwards whilst carrying water vapour, condensing into visible clouds. This circulation is organised into parallel rotating parallel columns of air, forming distinct cloud streets.

The central focus of this thesis is on the investigation of fluid behaviour arising from the interaction between shear and buoyancy forces, a common thread among the physical examples discussed above. We note that by isolating our analysis to the interaction between shear and buoyancy forces, we might neglect other physical mechanisms such as phase change, chemical reactions and evaporation, which may be significant in the context of cooling microprocessors, chemical vapour deposition, and atmospheric boundary layers respectively ([Vallis, Parker, & Tobias, 2019](#)). Nonetheless, the interaction between shear and buoyancy forces remains an open topic and will be the primary focus of this thesis, providing a foundation for future investigations that may include addition mechanisms.

To consider this interaction, we consider an idealised setup, known as the Rayleigh-Bénard-Poiseuille (RBP) flow. This RBP system describes the fluid motion confined between two infinitely extended parallel plates, heated from below and cooled from the top, with an additional pressure gradient driving the flow. The RBP configuration combines the two paradigmatic flow configurations; the classical Rayleigh-Bénard convection (RBC) and plane Poiseuille flow (PPF), driven by buoyancy and shear, respectively. While the onset of convection in RBC, and the transition to subcritical shear-driven turbulence in PPF have been both extensively studied, the transitional regime in which both forces interact remains less understood. Understanding their transitional behaviour and transport properties could have direct implications for the physical examples mentioned above.

The RBP configuration is illustrated in figure 1.1, where  $z, y, x$  refer to spatial coordinates denoting the streamwise, spanwise and wall normal directions.  $L_z, L_x, d$  and  $h$  corresponds to the length, span, depth and half-height of the domain respectively. The RBP system is biperiodic along  $z$  and  $x$ . The flow is driven by a pressure gradient along the streamwise  $z$  direction,  $\Delta P = P|_{z=0} - P|_{z=L_z} < 0$ , leading to a laminar Poiseuille flow,  $w(y) = W_c(1 - y^2)$ , where  $W_c$  is the laminar centerline velocity.

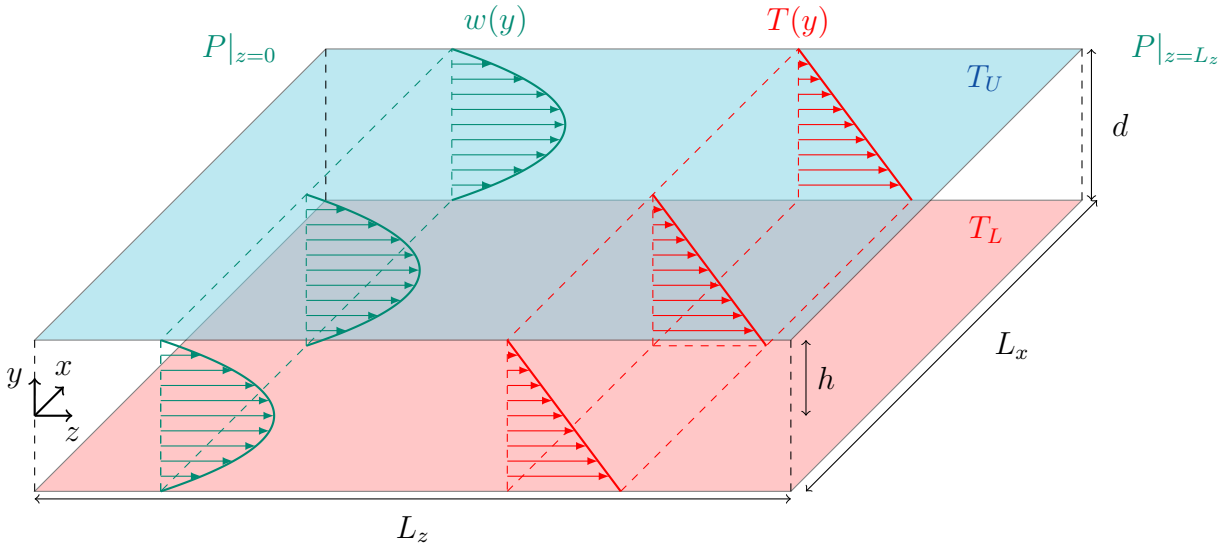


Figure 1.2: The Rayleigh-Bénard Poiseuille (RBP) flow configuration.

We consider a fully developed flow, where the boundary layer developing from the top and the bottom wall meets at the midplane  $y = 0$  and entrance effects are therefore neglected. Like the RBC system, the RBP system is unstably stratified. The temperature difference between the lower,  $T_L$ , and upper wall,  $T_U$ , is always positive,  $\Delta T = T_L - T_U > 0$ , leading to a stable linear conduction layer along the wall-normal direction,  $T(y)$ , if  $\Delta T$  is kept sufficiently small. The behaviour of RBP flows is governed by four dimensionless parameters,

$$Re = W_c h / \nu, \quad Ra = \frac{\eta g d^3 \Delta T}{\nu \kappa}, \quad Pr = \frac{\kappa}{\nu}, \quad \Gamma = L/2d, \quad (1.1)$$

where  $Re$ ,  $Ra$ ,  $Pr$ ,  $\Gamma$  refers to Reynolds, Rayleigh, Prandtl numbers and aspect ratio and  $\eta$ ,  $g$ ,  $\nu$ ,  $\kappa$ , are the thermal expansion coefficient, acceleration due to gravity, kinematic viscosity, thermal diffusivity, respectively. The Reynolds number,  $Re$ , and the Rayleigh number,  $Ra$ , are dimensionless parameters that characterise the relative influence of shear and buoyancy respectively. For sufficiently large values of  $Re$  and  $Ra$ , RBP flows may undergo a transition to shear-driven turbulence or convection-driven convection. In the absence of shear,  $Re = 0$ , the RBP configuration reduces to the classical buoyancy driven Rayleigh-Bénard convection, which forms a bistable system between stationary and chaotic convection rolls slightly above the critical  $Ra$ . The influence of  $Re$  on bistability remains unexplored.

In the first part of this thesis, we focus on the transitional regime by investigating whether buoyancy forces promote the transition to shear-driven turbulence and examining the effect of shear on convection in large domains. The second part of this thesis explores the state space structure of a bistable system between a chaotic convection roll state and a stationary convection roll state (see spiral defect chaos and ideal straight rolls in §1.3) of Rayleigh-Bénard convection.

The structure of this introductory chapter is as follows: we begin our discussion on the development of hydrodynamic stability theory of wall-bounded shear flows in §1.2. Theoretical frameworks used in the study of the stability of fluid flow, including linear modal/non-modal stability, nonlinear dynamical systems and the spatio-temporal dynamics of transitional shear flows will be discussed. Throughout

§1.2, we apply these concepts in the context of plane Poiseuille flows (PPF). This followed by the developments of Rayleigh-Bénard convection (RBC) in §1.3. Finally, we review the developments in RBP flows §1.4, before concluding this chapter with an outline of the thesis in §1.5.

## 1.2 Transitional wall-bounded shear flows

Wall-bounded shear flows concerns the motion of the fluid flowing in parallel to walls, typically bounded by one or more walls. Near the wall, the fluid comes to rest due to the no-slip boundary condition, resulting in a velocity gradient perpendicular to the wall, giving rise to shear within the fluid, commonly known as *wall-bounded shear flows*. Examples include the pressure-driven plane Poiseuille flow (channel flow), Hagen-Poiseuille flow (pipe flow), plane Couette flow and flat plate boundary layers. These geometrically simple configurations provides a convenient framework amenable to the mathematical analysis of fluid motion subjected to shear. Depending on the degree of shear, the fluid motion can be either laminar, where the fluid layers move in smooth parallel 'laminates', or turbulent, characterised by chaotic eddying motions. We also note that there is a transitional regime where both states can coexist discuss later. A central question is predicting the transition from the laminar regime to the turbulence.

The first investigation into this transition was conducted by [Reynolds \(1883\)](#). In his experimental setup, the flow speed through the pipe could be controlled by regulating the inlet pressure, while injecting dye to visualise the flow, as illustrated in figure 1.3(a). At low speeds, the fluid remained laminar, resulting to a single streak of steady dye in figure 1.3(b). As the speed increased, the dye begin to exhibit irregular 'sinuous' motions interspersed with laminar regions shown in figure 1.3(c). This is now referred to as the transitional regime, alternating between the laminar and turbulent states. Beyond a critical speed, the dye breaks down entirely into chaotic 'eddies', mixing with the surrounding fluid and discolouring the flow with dye downstream in figure 1.3(d). This regime is now identified as turbulence.

Reynolds proposed that the threshold between the laminar, transitional and turbulent regimes could be characterised by a non-dimensional parameter, now referred to as the Reynolds number,

$$Re = UD/\nu, \quad (1.2)$$

where  $U$  is the centerline velocity in the pipe,  $D$ , the pipe diameter and  $\nu$ , the kinematic viscosity. He observed that flow through the pipe remained *stable* and laminar for  $Re < 1900$ , while it became *unstable* and turbulent for  $Re > 2000$  ([Reynolds, 1895](#)), introducing the notion of flow *stability*.

### 1.2.1 Linear Stability Analysis

Following Reynolds' experiment, interest towards the mathematical analysis of the stability of laminar flows grew in early 20<sup>th</sup> century. The mathematical approach typically begins by decomposing the velocity field,  $\mathbf{u}(\mathbf{x}, t)$ , into a laminar (base) state,  $\mathbf{U}(y)$ , and the velocity perturbations,  $\mathbf{u}'(\mathbf{x}, t)$ , with

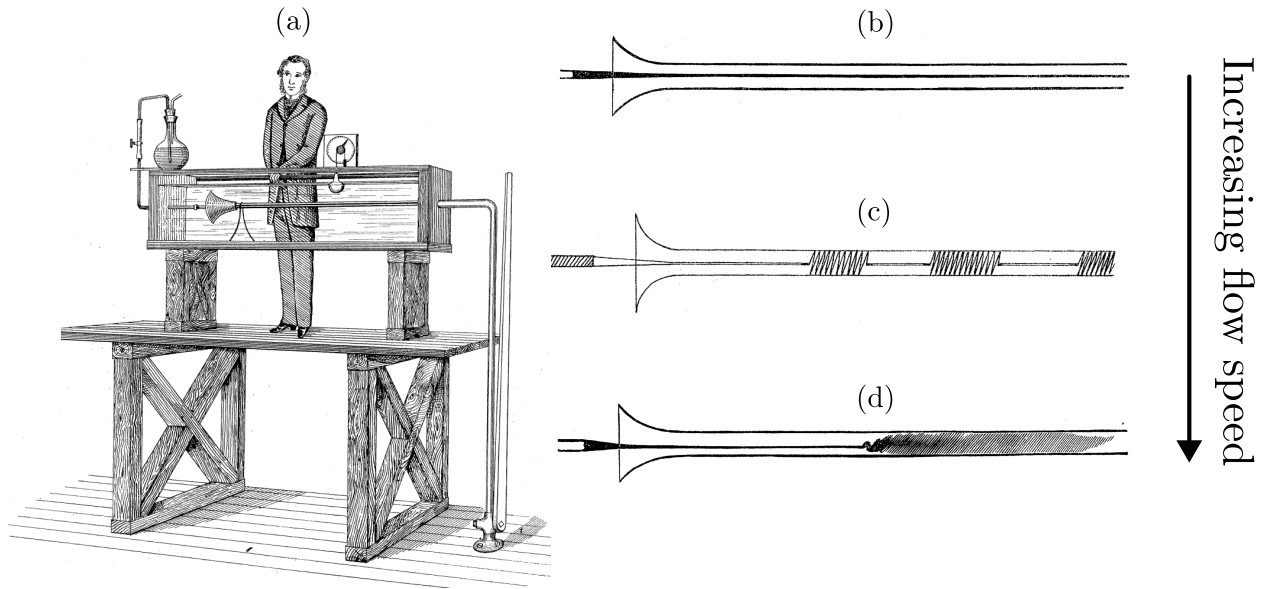


Figure 1.3: (a) Osbourne Reynolds pipe experiment with the dye injection apparatus, illustrating the (b) laminar flow, (c) transitional regime and (d) turbulent flow as the flow speed is increased, taken from [Reynolds \(1883\)](#).

pressure similarly decomposed as,

$$\mathbf{u}(\mathbf{x}) = U(y) + \mathbf{u}'(\mathbf{x}, t), \quad \text{and} \quad p(\mathbf{x}, t) = P(x) + p'(\mathbf{x}, t). \quad (1.3)$$

Substituting into the Navier-Stokes equations and linearising (neglecting nonlinear terms), we get,

$$\frac{\partial \mathbf{u}'}{\partial t} + (U \cdot \nabla) \mathbf{u}' + (\mathbf{u}' \cdot \nabla) U = -\nabla p' + \frac{1}{Re} \nabla^2 \mathbf{u}', \quad (1.4a)$$

$$\nabla \cdot \mathbf{u}' = 0, \quad (1.4b)$$

known as the linearised Navier-Stokes equations. This commonly followed by introducing a wavelike ansatz (mode) for the perturbations, and analysed by considering their behaviour independently, referred to as modal analysis in §1.2.1, or their coupled dynamics, referred to as non-modal analysis in §1.2.1.

### Modal analysis

It is convenient to eliminate the pressure terms by reformulating equation (1.4) using the wall-normal perturbation velocity,  $v'$ , and wall-normal vorticity,  $\eta' = \partial u'/\partial z - \partial w'/\partial x$ , variables. Using  $(v, \eta)$ , we introduce a modal ansatz for them,

$$v'(\mathbf{x}, t) = \tilde{v}(y) e^{i(\alpha x + \beta z - \omega t)}, \quad \text{and} \quad \eta'(\mathbf{x}, t) = \tilde{\eta}(y) e^{i(\alpha x + \beta z - \omega t)}. \quad (1.5)$$

where  $\alpha, \beta, \omega$  denotes the streamwise and spanwise wavenumbers, and complex frequency (i.e.  $\omega = \omega_r + i\omega_i$ ), respectively. Substituting this ansatz into linearised equations lead to the classical Orr-

Sommerfeld and Squire equations ([Orr, 1907](#); [Schmid & Henningson, 2001](#); [Sommerfeld, 1909](#); [Squire, 1933](#)),

$$\begin{pmatrix} \mathcal{L}_{OS} & 0 \\ i\beta U' & \mathcal{L}_{SQ} \end{pmatrix} \begin{pmatrix} \tilde{v} \\ \tilde{\eta} \end{pmatrix} = i\omega \begin{pmatrix} k^2 - \mathcal{D}^2 & 0 \\ 0 & 1 \end{pmatrix} \begin{pmatrix} \tilde{v} \\ \tilde{\eta} \end{pmatrix}. \quad (1.6a)$$

with

$$\mathcal{L}_{OS} = i\alpha U(k^2 - \mathcal{D}^2) + i\alpha U'' + \frac{1}{Re}(k^2 - \mathcal{D}^2)^2, \quad \mathcal{L}_{SQ} = i\alpha U + \frac{1}{Re}(k^2 - \mathcal{D}^2). \quad (1.6b)$$

where  $\mathcal{D} = d/dy$ ,  $k^2 = \alpha^2 + \beta^2$  and  $U''$  is the second derivative of  $U(y)$ . Equation (1.6a) is a generalised eigenvalue problem with eigenvalue  $i\omega$ , which determines the growth of perturbations.

The goal of modal stability analysis is to determine the critical Reynolds number  $Re_c$ , defined as the lowest value of  $Re$ , for all  $\alpha$  and  $\beta$  in which  $\Im[\omega] = 0$ . For  $Re > Re_c$ , perturbations can grow exponentially, indicating instability. Squire's theorem states that for every unstable three-dimensional perturbation, there exist an unstable two-dimensional perturbation, with a lower  $Re_c$  ([Squire, 1933](#)). This implies that the most linearly unstable perturbation of wall-bounded flows is two dimensional. Calculations by [Tollmien \(1928\)](#) and [Schlichting \(1933\)](#) for a flat-plate boundary layer flow yielded a critical Reynolds number based on displacement thickness,  $\delta^*$ , of  $Re_{ind} = U_\infty \delta^* / \nu = 520$ <sup>1</sup> ([Schlichting & Gersten, 2017](#)). These two dimensional unstable eigenmodes are known as Tollmien-Schlichting (T.S) waves. In plane Poiseuille flow, the critical Reynolds number is  $Re_c = 5772.2$  with a critical wavenumber of  $\alpha_c = 1.02$  ([Orszag, 1971](#)). However, experiments reveal that transition to turbulence can occur at a lower Reynolds number, around,  $Re \sim 1000 - 2000$  ([Davies & White, 1928](#); [Dean, 1978](#); [Iida & Nagano, 1998](#); [Patel & Head, 1969](#); [Tsukahara, Iwamoto, Kawamura, & Takeda, 2014](#)), highlighting a key limitation of modal analysis. Similar discrepancies are observed in plane Couette and pipe flows ([Meseguer & Trefethen, 2003](#)), where the laminar state is linearly stable for all  $Re$ , yet transition to turbulence occurs. Despite these limitations, modal analysis predicts instabilities in other systems such as Rayleigh-Bénard convection and Taylor-Couette flow ([Chandrasekhar, 1968](#)). Further extensions of modal stability, including spatial instability analysis ([Huerre & Monkewitz, 1990](#)), and secondary instability ([Orszag & Patera, 1983](#)) are well established and are beyond the scope of this thesis.

## Non-modal stability

One of a major limitations of modal analysis is that it treats each eigenmode independently. However, the interaction between decaying eigenmodes can lead to a transient growth, where perturbations amplify temporarily before decaying asymptotically. To demonstrate an example of transient growth, we consider a two-dimensional toy model governing the time-evolution of  $\mathbf{q} = (v, \eta)^T$ ,

$$\frac{d}{dt} \begin{pmatrix} v \\ \eta \end{pmatrix} = \begin{pmatrix} -\frac{1}{Re} & -1 \\ 0 & -\frac{2}{Re} \end{pmatrix} \begin{pmatrix} v \\ \eta \end{pmatrix}, \quad (1.7)$$

---

<sup>1</sup>In the literature of stability theory,  $Re_{ind}$  refers to the indifference Reynolds number which is similar to the critical Reynolds number,  $Re_c$ . However, boundary layer transition often takes place over a finite distance, and the indifference point is used to disambiguate between the onset of transition and the critical point of completed transition.

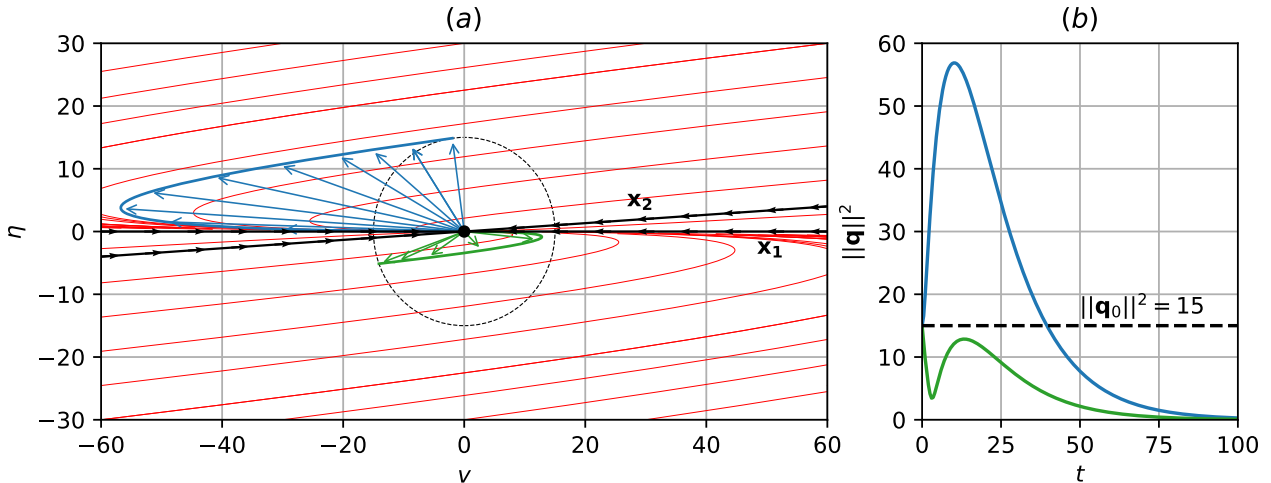


Figure 1.4: (a) The phase portrait of the toy model with  $Re = 15$ , where red lines are phase lines of the toy model. The blue trajectory lead to transient growth and the green trajectory do not (b) Time history of blue and green trajectory.

where  $Re$  refers to the Reynolds number. The toy model has negative eigenvalues,  $(\lambda_1, \lambda_2) = (-1/Re, -2/Re)$ , indicating asymptotic decay. At  $Re = 15$ , the eigenvectors,  $\mathbf{x}_1 = (1, 0)$ ,  $\mathbf{x}_2 = (1, \frac{1}{\sqrt{Re^2+1}})$ , are highly non-orthogonal, becoming almost parallel shown in figure 1.4(a). Notably, they become increasingly linearly dependent as  $Re \rightarrow \infty$ . For a particular initial condition, the energy  $\|q\|^2 = \sqrt{v^2 + \eta^2}$ , is amplified four times before decaying in blue trajectory, shown in Figure 1.4(b). Yet for another choice of initial condition, the trajectory decays asymptotically as the green trajectory indicates. Despite decaying eigenmodes, the toy model highlights the significance of transient growth, which depends on the choice of initial condition.

The aim of non-modal stability analysis is to search for optimal initial conditions,  $\tilde{\mathbf{q}}_0$ , that leads to the maximum amplification,  $G(\tau)$ , over a time horizon  $\tau$ . This is posed as an optimistaion problem,

$$G(\tau) = \max_{\tilde{\mathbf{q}}_0 \neq 0} \frac{\langle \tilde{\mathbf{q}}(\tau), \tilde{\mathbf{q}}(\tau) \rangle}{\langle \tilde{\mathbf{q}}_0, \tilde{\mathbf{q}}_0 \rangle}, \quad \text{s.t. } \langle \tilde{\mathbf{q}}_0, \tilde{\mathbf{q}}_0 \rangle = 1, \quad (1.8)$$

where,  $\langle \cdot, \cdot \rangle$  denotes the inner-product,

$$\langle \tilde{\mathbf{q}}, \tilde{\mathbf{q}} \rangle = \int_{\Omega} \tilde{\mathbf{q}}^H \tilde{\mathbf{q}} d\Omega, \quad (1.9)$$

and  $\tilde{\mathbf{q}}^H$  refers to the complex conjugate transpose of  $\tilde{\mathbf{q}}$ . By considering the linearised operator of (1.6a), we define a linear operator as,

$$\tilde{\mathbf{q}}(\tau) = \mathcal{A}(\tau) \tilde{\mathbf{q}}_0, \quad (1.10)$$

which takes the solution from initial conditions,  $\tilde{\mathbf{q}}_0$ , to  $\tilde{\mathbf{q}}(\tau)$  at time  $\tau$ . Subtituting the expression above into equation (1.8),

$$G(\tau) = \max_{\tilde{\mathbf{q}}_0 \neq 0} \frac{\langle \mathcal{A}(\tau) \tilde{\mathbf{q}}_0, \mathcal{A}(\tau) \tilde{\mathbf{q}}_0 \rangle}{\langle \tilde{\mathbf{q}}_0, \tilde{\mathbf{q}}_0 \rangle} = \langle \tilde{\mathbf{q}}_0, \mathcal{A}^\dagger(\tau) \mathcal{A}(\tau) \tilde{\mathbf{q}}_0 \rangle = \lambda_{max}(\mathcal{A}(\tau)^\dagger \mathcal{A}(\tau)), \quad (1.11)$$

where  $\mathcal{A}^\dagger$  refers to the adjoint of  $\mathcal{A}(t)$ . The maximum amplification factor  $\max G(t)$  is the largest eigenvalue of  $\mathcal{A}^\dagger(\tau)\mathcal{A}(\tau)$ . The eigenvalue problem is given as,

$$\mathcal{A}^\dagger(t)\mathcal{A}(t)\tilde{\mathbf{q}}_0 = \lambda\tilde{\mathbf{q}}_0, \quad (1.12)$$

where  $\tilde{\mathbf{q}}_0$  refers to the eigenvector denoting the optimal initial condition. For a detailed derivation of the optimal initial conditions or forcing, the reader is referred to [Butler and Farrell \(1992\)](#) and [Schmid \(2007\)](#). An alternative method of computing the optimal transient growth is by analysing the pseudospectral of linear operators discussed by [Trefethen \(1997\)](#).

Both two-, and three-dimensional non-modal analyses reveal mechanisms for transient growth. In two-dimensions, the optimal initial conditions are in the form of near wall vortices tilted upstream, which amplifies transiently via the Orr-mechanism ([Farrell, 1988](#); [Orr, 1907](#); [Reddy, Schmid, & Henningson, 1993](#)). In three-dimensions, streamwise vortices are optimal, leading to the the amplification of streamwise streaks via the well known lift-up effect ([Ellingsen & Palm, 1975](#); [Reddy & Henningson, 1993](#)). Notably, the spacing of these streaks analysed using non-modal analysis at higher Reynolds number has been consistently reported to occur around 100 wall units ([Del Álamo & Jiménez, 2006](#); [Hwang & Cossu, 2010](#); [Pujals, García-Villalba, Cossu, & Depardon, 2009](#)), which supports experimental observations of streak spacing in turbulent boundary layers ([Kline, Reynolds, Schraub, & Runstadler, 1967](#); [Smith & Metzler, 1983](#)).

The main results from non-modal analysis is that three dimensional perturbations can lead to strong transient growth at subcritical Reynolds numbers, contradicting the two dimensional TS waves from modal analysis. Both modal and non-modal mechanisms highlight important insights into the linear mechanisms which might be responsible for the transition from laminar to turbulent flows.

## 1.2.2 Nonlinear dynamical systems

In the previous section, we have examined the laminar to turbulent transition using linear frameworks. However, the the transition process is ultimately described by the nonlinear Navier-Stokes equations, which motivates the development and adoption of mathematical frameworks beyond linear methbods.

In the context of shear flow turbulence, there has been a growing interests in adopting techniques from nonlinear dynamical systems, interpreting turbulence as a chaotic trajectories which evolves within a finite-dimensional phase space. This phase space refers to a set of solutions satisfying the Navier-Stokes equations, first conjectured to be infinite dimensional by [Hopf \(1948\)](#). He postulated that within the infinite dimension phase space lie a finite dimensional manifold, whose properties depended on viscosity. For large viscosities (i.e. low  $Re$ ), this finite dimensional space corresponds to a single point, the laminar state. This point may become linearly unstable at a certain critical Reynolds number, bifurcating to form new manifolds, as viscosity is decreased (i.e.  $Re$  is increased) further, potentially leading to chaos. The set of such manifolds is referred to *inertial manifolds*, and its existence under certain properties has been established ([Foias, Sell, & Temam, 1988](#)). An implication of this is that the transition to turbulence could be viewed as successive bifurcations from the laminar state, govern by a single control parameter (i.e. the Reynolds numnber), generalised by the so called

routes to chaos scenarios.

Landau (1944) proposed that the transition to turbulence may occur through a sequence of Hopf bifurcations, each introducing a new incommensurate frequency, resulting in quasi-periodic motions on a high-dimensional torus. However, this model did not capture the essential ingredients of turbulence, such as sensitivity of initial conditions and mixing (John, Gunter, & Maria, 1993). Ruelle and Takens (1971) later show that a *strange attractor*, exhibit the key features of chaos, can emerge after three successive Hopf bifurcations from a stationary state, referred to as the *Ruelle-Takens* route to chaos. This scenario has been observed in Taylor-Couette flow (Gollub & Swinney, 1975), and Rayleigh-Bénard convection (Swinney & Gollub, 1978). Other routes to chaos scenarios, such as periodic-doubling (Feigenbaum, 1979), and intermittency (Manneville & Pomeau, 1979) scenarios have been proposed. For a review of these routes to chaos scenarios, the reader is referred to John et al. (1993). Nonetheless, the transition to turbulence is subcritical in shear flow configurations, meaning that the route of chaos scenarios do not necessarily apply through bifurcations from the laminar state.

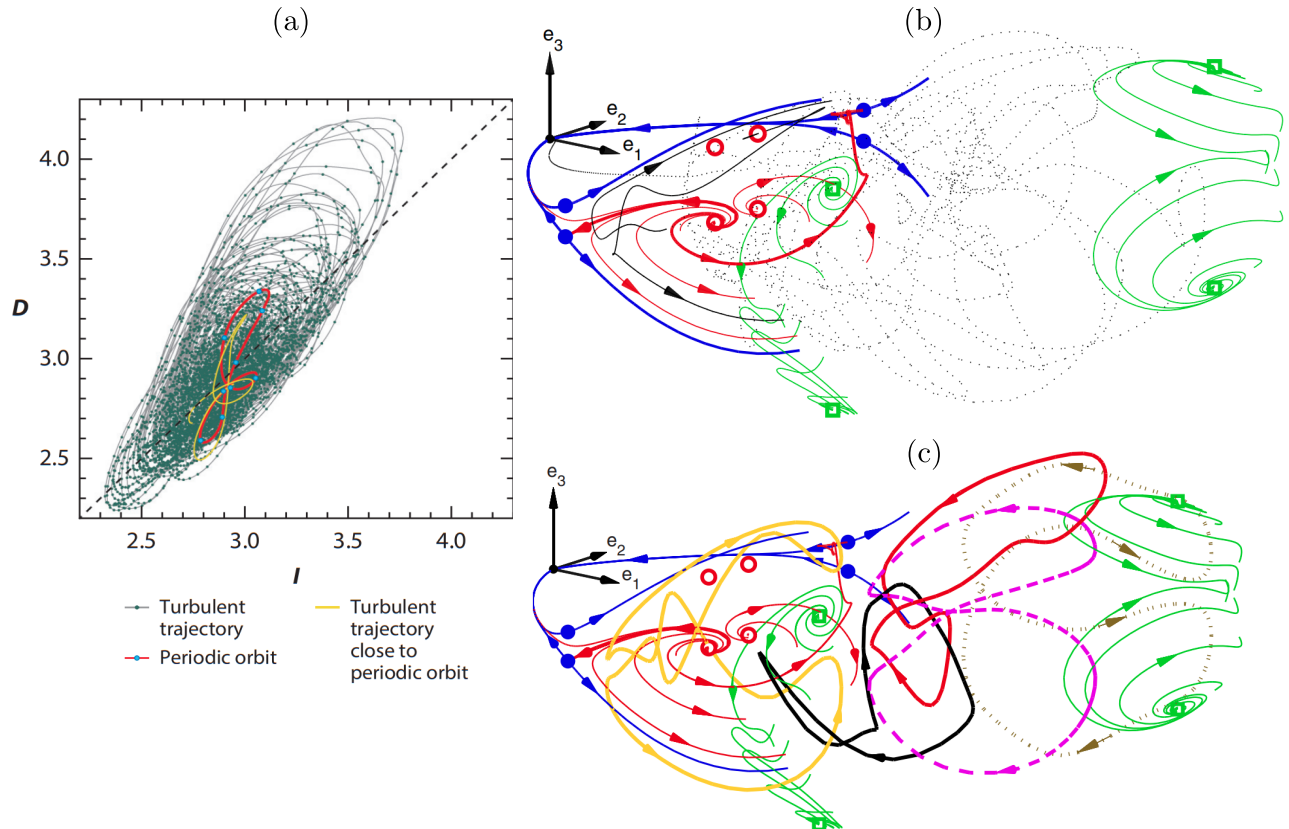


Figure 1.5: (a) Chaotic trajectories of plane Couette flow at  $Re = 400$ , approaching an unstable periodic orbit (red) highlighted as yellow, adopted from Kawahara and Kida (2001). (b) State space organisation of turbulence trajectories (black dots) confined around equilibria (circles, dots and squares) and their unstable manifolds (solid lines), heteroclinic connections between them are shown in red. The coordinate system,  $(e_{1,2,3})$ , is centered on the laminar state, using a linear combination of the upper branch invariant state. (c) State space projection of five periodic orbits (coloured solid lines), embedded within the same space where turbulence evolves in (b), adopted from Cvitanović and Gibson (2010).

A major development came with the identification of a pair of non-trivial, unstable equilibrium states in plane Couette flow (Nagata, 1990). This pair referred to as the *lower* and *upper* branches,

emerging from a saddle node bifurcation disconnected from the stable laminar state. The *lower* branch lies closer to the laminar state, while the *upper* branch resides further away in state space. Later, a travelling-wave solution in plane Couette flow also later found by the same author (Nagata, 1997). A family of equilibrium and travelling-wave solutions was found later for plane Couette and plane Poiseuille flows under different boundary conditions (i.e. stress-free, slip and no-slip) were identified by (Waleffe, 2001, 2003). Additional equilibria and travelling-wave solutions were identified by Gibson, Halcrow, and Cvitanović (2008, 2009), along with their heteroclinic connections between them (Halcrow, Gibson, Cvitanović, & Viswanath, 2009). In the context of pipe flow, multiple travelling-wave solutions have also been reported (Duguet, Willis, & Kerswell, 2008; Faisst & Eckhardt, 2003; Kerswell & Tutty, 2007; Pringle, Duguet, & Kerswell, 2009; Wang, Gibson, & Waleffe, 2007; Wedin & Kerswell, 2004). The set of equilibria, and travelling waves, shows good agreement with the statistical quantities (e.g. mean and fluctuations) with direct numerical simulations. However, since they time independent (within a moving reference frame for travelling waves), they do no capture the temporal dynamics of turbulence such as the *self-sustaining process* (SSP) (Hamilton, Kim, & Waleffe, 1995) (see §1.2.3). While these unstable solutions demonstrate good agreements with results from DNS such as the spanwise length scales, and mean and fluctuations, they do not capture the dynamical processes.

The next breakthrough was on the identification of time-dependent unstable solutions in the form of periodic orbits. Kawahara and Kida (2001) computed a pair of periodic orbits in plane Couette, with one exhibiting a single regeneration cycle similar to the SSP (see figure 1.5(a)) while the other exhibits mild modulation of streaks. These periodic orbits are linked by heteroclinic connections. In plane Poiseuille flow, Toh and Itano (2003) also identified periodic orbits displaying bursting behaviour. Using a Newton–Krylov iteration with a hook-step modification, Viswanath (2007) computed multiply relative periodic orbits. These studies conceptualise that the chaotic trajectories of turbulence as being embedded within a set of unstable periodic orbits, evolving along their unstable manifolds (Gibson et al., 2008, 2009; Graham & Floryan, 2021; Halcrow et al., 2009; Viswanath, 2007). An example is shown in figure 1.5, where the chaotic trajectories in figure 1.5(b), reside within the same state space as the periodic orbits, enclosed by equilibria and their heteroclinic connections shown in figure 1.5(c). The set of equilibria, travelling waves and their relative counterparts, are referred to as *invariant solutions* offering a building block description of turbulence. However, they do not provide insight into the transition process, since these solutions already reside in the turbulent attractor.

The transition to turbulence in canonical shear flow configurations are typically subcritical, emerging from the invariant solutions described above, accompanied by an underlying stable laminar state. A consequence of this is that the laminar and turbulent states form a bistable attractors in phase space with a boundary, separating their respective basins of attraction known as the *edge*. Attractors that sit along this edge have been identified and found to possess a saddle-like structure, attracting trajectories within the edge and repelling them toward either the laminar or turbulent state, known as *edge* states. The bisection algorithm used for edge tracking, was first employed in pipe flow experiments by Schneider, Eckhardt, and Yorke (2007), was identified to be chaotic. Time-averaging of this chaotic attractor revealed a close resemblance to the unstable lower branch travelling-wave

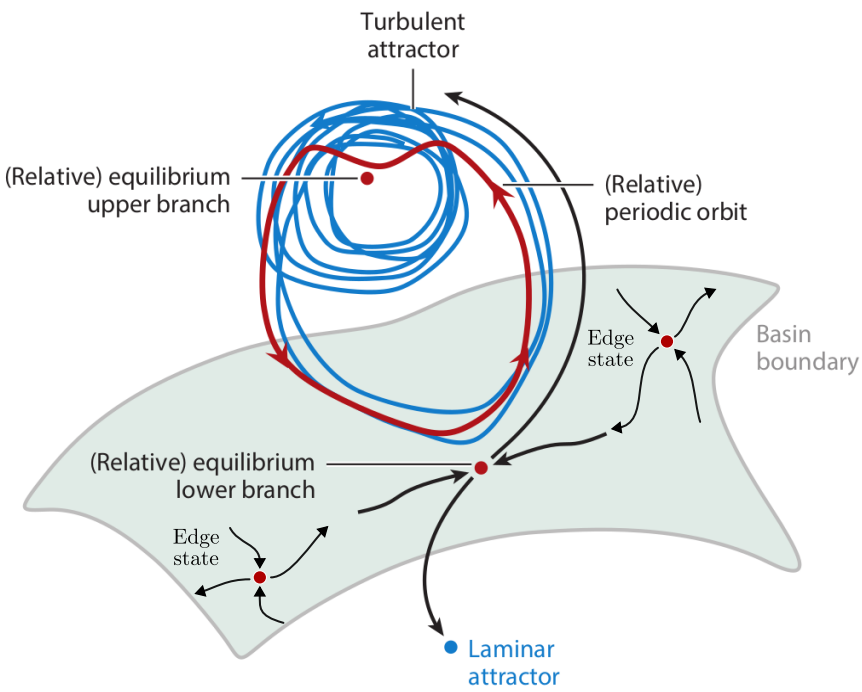


Figure 1.6: A graphical representation of the edge (grey surface) separating the basin of boundary of the laminar and turbulent attractor, consisting of attractors, known as edge states, adapted from [Graham and Floryan \(2021\)](#).

solutions, suggesting that the edge separating basin of attraction between the laminar and turbulent states consist of the lower branch solutions and their symmetries ([Duguet et al., 2008; Pringle et al., 2009](#)). As Reynolds number increases, the edge and the turbulent attractor moves apart ([Schneider & Eckhardt, 2009](#)). In the context of pipe flows, it was recognised that the edge consists of a set of unstable lower branch travelling-wave solutions. A graphical representation of the edge, and edge states, separating the laminar the turbulent states is shown in figure 1.6. Near the onset of subcritical turbulence, turbulence appear to be transient, decaying towards the laminar solution after a finite lifetime ([Bottin, Daviaud, Manneville, & Dauchot, 1998; Faisst & Eckhardt, 2004; Hof, Westerweel, Schneider, & Eckhardt, 2006](#)) This can be interpreted as the turbulent chaotic attractor colliding with the lower branch solution through a *boundary crisis* ([Lai & Tél, 2011](#)), forming a chaotic saddle where solution trajectories may ‘leak’ (relaminarise) towards the laminar state ([Kreilos & Eckhardt, 2012; Mellibovsky & Eckhardt, 2012; Zammert & Eckhardt, 2015](#)). The onset a boundary crisis (transient turbulence) have been also attributed to the emergence of homoclinic tangency in plane Couette flow ([Lustro, Kawahara, Van Veen, Shimizu, & Kokubu, 2019; Van Veen & Kawahara, 2011](#)).

### 1.2.3 Self-sustaining process

The self-sustaining process (SSP) describe the dynamical interaction between a pair of streaks and quasi-streamwise vortices, considered to be the fundamental process of wall bounded turbulent flows in the near wall region. It is defined by a quasi-cyclic process, consisting of three distinct phases: (1) the formation of streamwise streaks due to a linear advection by streamwise vortices, (2) the wavy

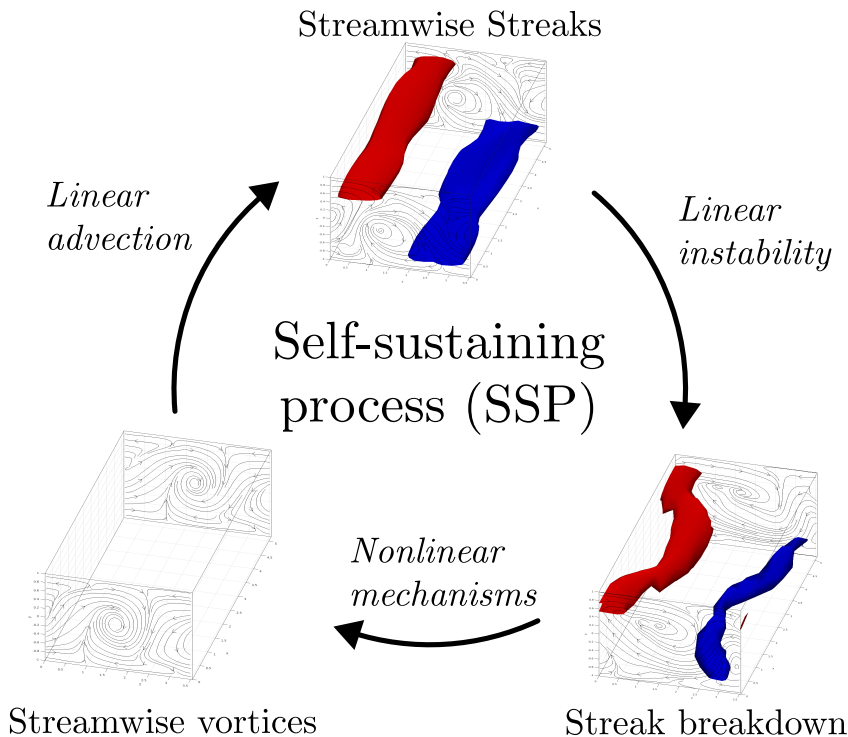


Figure 1.7: The self-sustaining process, consisting of three phases: (1) Streak formation from linear advection by streamwise vortices, (2) streak breakdown due to streak instability and (3) regeneration of streamwise vortices via nonlinear mechanisms.

breakdown of streaks due to linear instability and (3) the regeneration of streamwise vortices via nonlinear mechanisms (Hamilton et al., 1995; Waleffe, 1997; Waleffe, Kim, & Hamilton, 1993). A schematic of the SSP is shown in figure 1.7. While early investigations of the SSP was confined the buffer layer (Hamilton et al., 1995), evidence that the SSP extends towards the logarithmic and outer region has been found (Cossu & Hwang, 2017). In parallel to the SSP, the vortex-wave interaction (VWI) theory developed to describe the sustained interactions between a general class of vortices and waves for asymptotically large Reynolds number (Hall & Smith, 1988, 1990, 1991), was found to be linked to the SSP (Hall & Sherwin, 2010). In particular, the solutions obtained using VWI theory by Hall and Sherwin (2010) is analogous to the lower branch solution from Wang et al. (2007).

#### 1.2.4 Spatiotemporal transitional flows

This section describes the inherent spatiotemporal structure of subcritical turbulence near the onset commonly reported in large extended domains. In this regime, turbulence is characterised by the coexistence of turbulent and laminar structures. Examples of such are found in canonical shear flow systems such as plane Couette flows (Barkley & Tuckerman, 2005, 2007; Duguet, Schlatter, & Henningson, 2010; Prigent, Grégoire, Chaté, & Dauchot, 2003; Reetz, Kreilos, & Schneider, 2019; Tuckerman & Barkley, 2011), Taylor-Couette flows (Prigent & Dauchot, 2002; Prigent et al., 2003), pipe flows (K. Avila et al., 2011; M. Avila, Barkley, & Hof, 2023; M. Avila, Willis, & Hof, 2010; Song, Barkley, Hof, & Avila, 2017) and plane Poiseuille flows (Gomé, Tuckerman, & Barkley, 2020; Paranjape, 2019; Paranjape, Duguet, & Hof, 2020; Paranjape, Yalniz, Duguet, Budanur, & Hof,

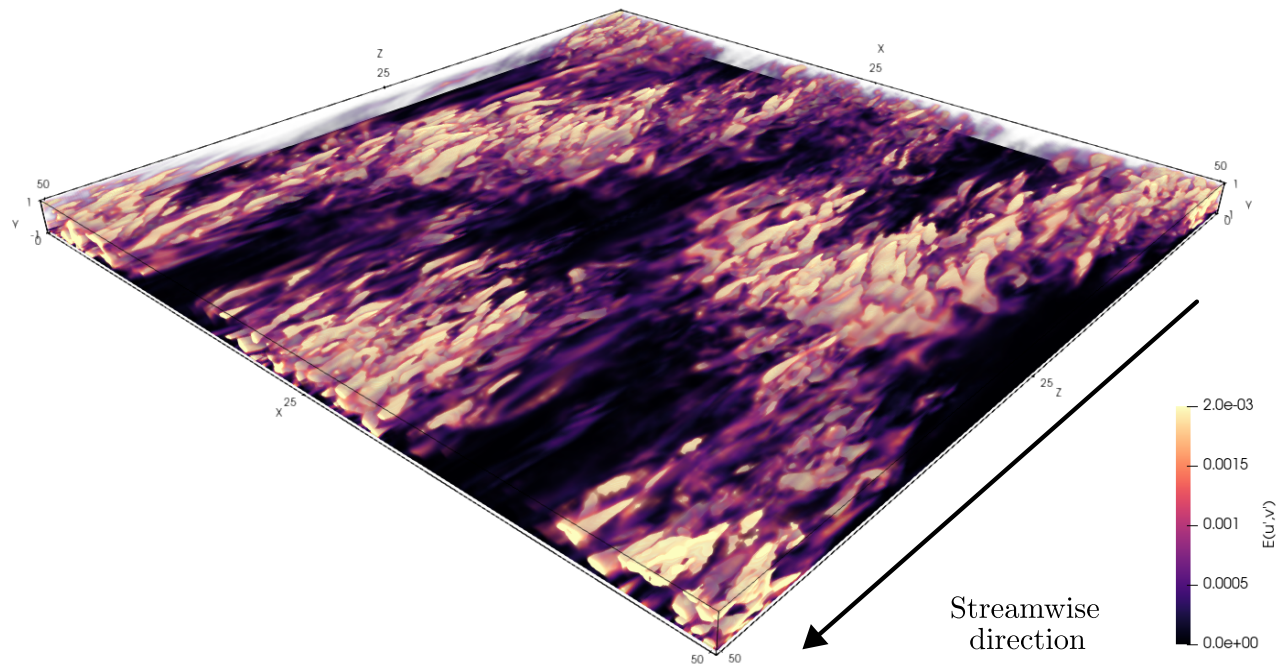


Figure 1.8: A snapshot of turbulent-laminar bands at  $Re = 1400$  in a large domain  $L/h = 16\pi$ , depicting its spatiotemporal intermittent nature. Isovolumetric renderings are based on the spanwise,  $u'$ , and wall-normal,  $v'$ , perturbation kinetic energy,  $E(u', v') = 1/2(u'^2 + v'^2)$ , where the perturbation velocities are defined about the laminar state  $\mathbf{u}'(\mathbf{x}, t) = \mathbf{u}(\mathbf{x}, t) - U_{lam}(y)$ .

2023; Tsukahara, Iwamoto, et al., 2014; Tsukahara, Kawaguchi, & Kawamura, 2014; Tsukahara, Seki, Kawamura, & Tochio, 2014; Tuckerman, Kreilos, Schröbsdorff, Schneider, & Gibson, 2014).

We will focus on the plane Poiseuille flow configuration, where the spatiotemporal intermittent patterns are referred to as oblique turbulent-laminar bands illustrated in figure 1.8 at  $Re = 1400$  for  $L/h = 16\pi$ . The bright and dark regions highlight coexisting spatially localised turbulent and laminar regions. These turbulent-laminar bands occur over a range of Reynolds numbers, and its precise range is dependent on the domain's aspect ratio (Paranjape et al., 2023; Tsukahara, Kawaguchi, & Kawamura, 2014; Tuckerman et al., 2014). Near the upper  $Re$  threshold of this regime, the domain is fully engulfed by uniform, featureless turbulence appearing at  $Re = 1800$  in figure 1.8(a). As  $Re$  decreases towards  $Re = 1050$ , spatiotemporal turbulent and laminar structures known as turbulent-laminar bands persist in between  $Re \in [1050, 1600]$  shown in figures 1.9(b-f). In particular, these turbulent-laminar appear to have a preferred inclined angle, between  $20^\circ \sim 30^\circ$ , with streamwise wavelengths of  $\lambda_x \sim 60h$ , and spanwise wavelengths of  $\lambda_z \sim 20h - 30h$  (Tsukahara, Kawaguchi, & Kawamura, 2014). Kashyap, Duguet, and Dauchot (2022) considered the linear response of the fluctuating turbulent field, and showed that the preferred band angle emerges near  $23.2^\circ$ . In the minimal band unit (MBU) studies of plane Poiseuille flows, the turbulent-bands convect at about  $\sim 1\%$  of the bulk velocity, propagating

either upstream or downstream, depending on  $Re$  (Gomé et al., 2020; Tuckerman et al., 2014). Notably, the spanwise lengths of the bands are much wider than the half-heights and depends on  $Re$ , appearing at  $\lambda_z \sim 20h$  for  $Re \gtrsim 1400$  and  $\lambda_z \sim 40h$  for  $Re \lesssim 1100$ . Interestingly, the bands alternate between both spanwise lengths between the  $Re$  range, merging and splitting continuously (Tuckerman et al., 2014), reminiscent of a puff splitting process in pipe flows (K. Avila et al., 2011). An example of this could have been observed in  $Re = 1050$ , where the band appears to alternate between different spanwise wavelengths in figure 1.9(f). As  $Re$  falls below a certain  $Re$  threshold, turbulent bands spontaneously decay and relaminarises (Gomé et al., 2020; Tuckerman et al., 2014). An example is shown in figure 1.9(g).

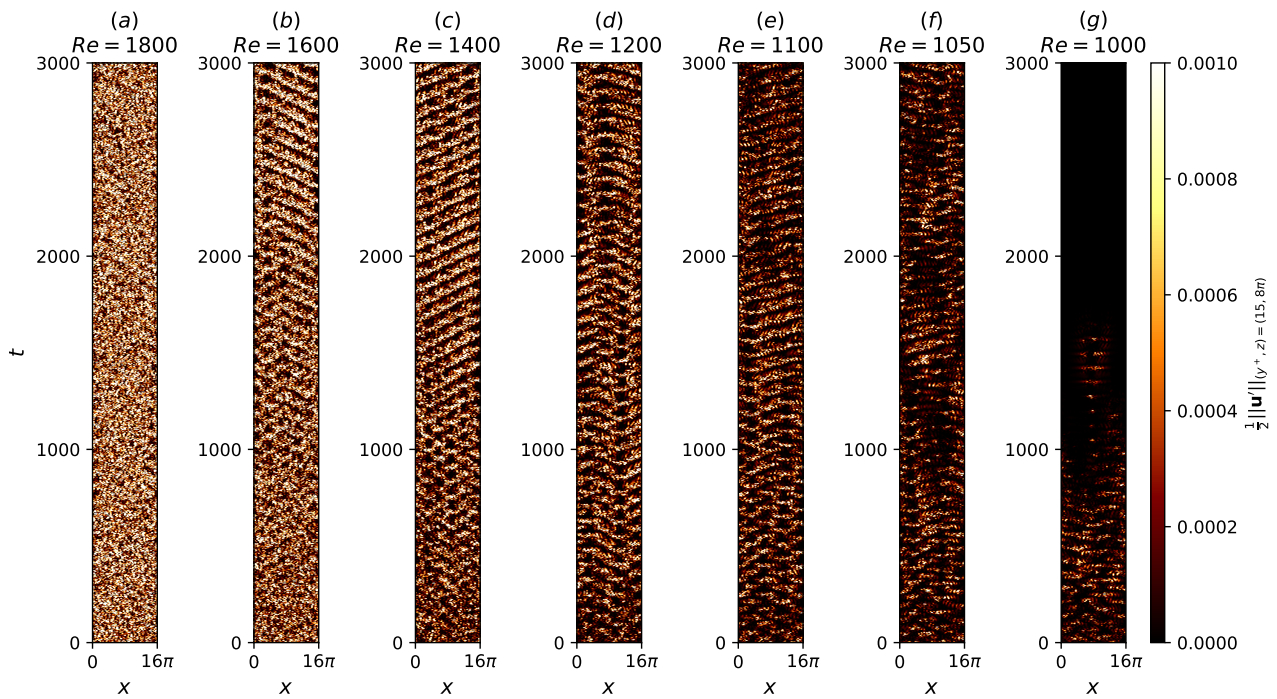


Figure 1.9: Turbulent-laminar bands for  $t \in [0, 3000]$  in large domains  $(L_x, L_z) = (16\pi, 16\pi)$  at (a)  $Re = 1800$ , (b)  $Re = 1600$ , (c)  $Re = 1400$ , (d)  $Re = 1200$ , (e)  $Re = 1100$ , (f)  $Re = 1050$ , (g)  $Re = 1000$ .

Gomé et al. (2020) computed the probability distributions for turbulent-laminar band decay,  $P(\Delta t^d)$ , where  $\Delta t^d$  is the time until decay. A key insight is that the probability distributions of turbulent band decay mimics a memoryless Poisson process,

$$P(\Delta t^d) = \exp(-\Delta t^d/\tau^d(Re)), \quad (1.13)$$

where  $\tau^d(Re)$  refers to the mean lifetime for decay as a function of  $Re$ . Similarly, the band splitting process also follows a Poisson process,

$$P(\Delta t^s) = \exp(-\Delta t^s/\tau^s(Re)), \quad (1.14)$$

with  $\tau^s(Re)$  the mean splitting lifetime. Both  $\tau^d$  and  $\tau^s$  exhibit superexponential dependence on  $Re$ ,

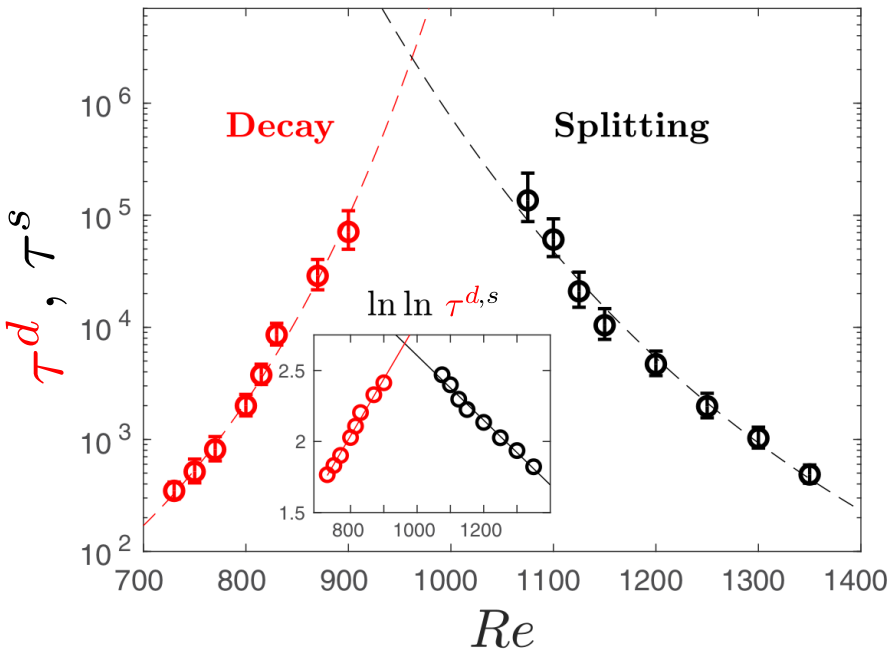


Figure 1.10: The mean decay times (red),  $\tau^d$ , and mean splitting times (black),  $\tau^s$ , as a function of Reynolds number, leading to a crossover point at  $Re_{cross} \approx 965$ , adapted from [Gomé et al. \(2020\)](#).

$$\tau^{d,s} = \exp(\exp(Re)), \quad (1.15)$$

This is shown in figure 1.10, with a crossover point at  $Re_{cross} \approx 965$ , where both decay and splitting becomes equally probable. This crossover point is considered as the critical Reynolds number for the onset of turbulent bands.

While there has been progress made towards our understanding of infinitely bi-periodic turbulent-laminar bands in MBUs, recent studies of isolated (non-periodic) turbulent bands (ITBs) reveal different behaviour. Notably, ITBs persist at Reynolds number below  $Re_{cross}$  at  $Re = 700$  for durations exceeding  $t = 10000$ , exceeding the mean decay lifetime in figure 1.10. The ITBs are characterised by streak generating head and a diffusive upstream tail. ([Shimizu & Manneville, 2019](#); [Tao, Eckhardt, & Xiong, 2018](#); [Xiao & Song, 2020](#); [Xiong, Tao, Chen, & Brandt, 2015](#)). We conclude our discussion on transitional wall-bounded shear flows.

## 1.3 Rayleigh-Bénard convection

Rayleigh-Bénard convection (RBC) is a paradigmatic fluid configuration describing the motion of the fluid confined between two infinite-parallel plates heated from below and cooled from the top. As the bottom plate is heated, the bottom layer fluid becomes more buoyant and tends to rise, while the colder top fluid layer becomes relatively less buoyant and tends to sink, leading to an overturning of layers. Viscous forces between neighbouring fluid parcels act to resist the motion. As buoyancy overcomes these viscous forces, the fluid layers overturn, resulting in the initiation of buoyancy-driven convection, the physical mechanism underpinning RBC.

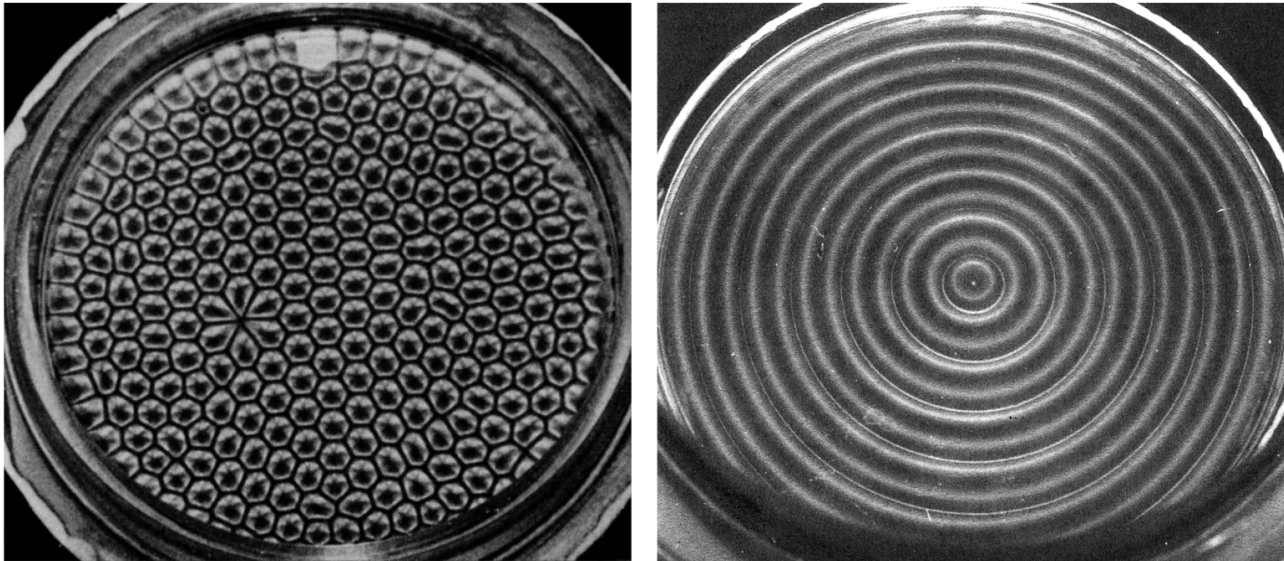


Figure 1.11: (a) Surface tension driven convection leading to the onset of hexagonal Bénard cells in a thin layer of silicone oil, heated from below and cooled by ambient air. A diamond defect appears, likely caused by plate imperfections. (b) Buoyancy driven convection in rigid plates, resulting to concentric convection rolls at 2.9 times the critical Rayleigh number. Both experiments were performed by [Koschmieder and Pallas \(1974\)](#), and the convection patterns were illuminated by aluminum powder, where the dark and bright regions refer to vertical and horizontal motions respectively. These higher resolution images were taken from [Van Dyke and Van Dyke \(1982\)](#).

One of the earliest experimental studies dedicated to buoyancy-driven convection was conducted by Henri Bénard ([Bénard, 1901](#)), who observed the formation of hexagonal convection cells above a certain temperature threshold  $\Delta T$ . These hexagonal patterns are referred to as Bénard cells are illustrated in figure 1.11(a) (adapted from ([Koschmieder & Pallas, 1974](#))). Subsequently, [Rayleigh \(1916\)](#) carried out one of first linear stability analyses of buoyancy-driven convection, predicting the onset of convection at a critical Rayleigh number of  $Ra_c = 657.5$ . However, Rayleigh's analysis assumed an idealised free-free boundary conditions, which differed from the rigid-free setup of Bénard's experiment. The linear stability analysis for rigid-free configuration was later performed by [Jeffreys \(1928\)](#) yielding a higher critical Rayleigh number of  $Ra_c = 1058$ . In the rigid-rigid configuration, the critical Rayleigh number increases further to  $Ra_c = 1708$  ([Pellew & Southwell, 1940](#)). The Rayleigh number in Bénard's original experiment contradicted results from linear stability analysis as it was found to be 300 to 1500 smaller than  $Ra_c$  for the free-free and rigid-free cases respectively ([Wesfreid, 2017](#)). This contradiction, not recognised by Bénard at the time, lies in the significant role of surface tension in thin fluid layers exposed to air, now known as Bénard-Maragoni (BM) convection ([Block, 1956](#); [Cloot & Lebon, 1984](#); [Manneville, 2006](#); [Wesfreid, 2017](#)). In BM convection, fluid motion is primarily driven by surface tension gradients due to variations of temperature, forming hexagonal cells, as in figure 1.11(a). The preference for hexagonal cells in BM convection was later confirmed based on weakly nonlinear stability analysis ([Cloot & Lebon, 1984](#)). As the fluid layer becomes thicker, surface-tension effects diminish and buoyancy-driven convection becomes dominant. Similarly, placing a rigid lid on top of a thin fluid layer suppresses surface-tension effects, resulting in buoyancy-driven convection (compare between 1.11(a) and (b)) The preferred

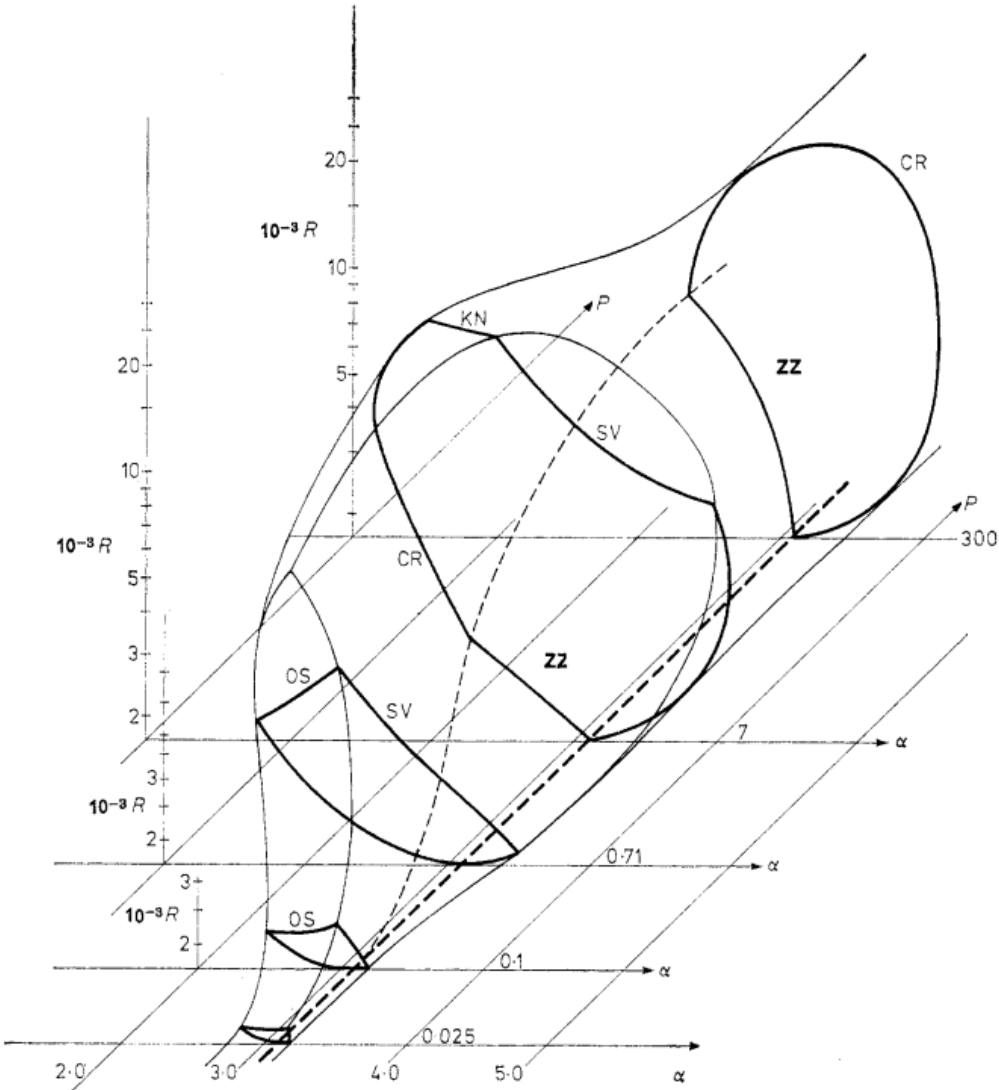


Figure 1.12: The Busse balloon describes the stability boundaries of ISRs in a  $\varepsilon - q$  space. For larger wavenumbers, the instability mechanism is described by the skewed-varicose (SV) instability. For smaller wavenumbers, the instability mechanism is described by the Eckhaus instability. For large  $\varepsilon$ , the instability is described by the onset of oscillatory instability. Busse balloon digitised from [Plapp \(1997\)](#) for  $Pr \approx 1$ .

convection patterns based on weakly nonlinear stability analysis are the two-dimensional parallel rolls, now referred to as ideal straight rolls (ISRs) ([Bodenschatz, Pesch, & Ahlers, 2000](#); [Schlüter, Lortz, & Busse, 1965](#)). In circular containers, the ISRs conform to the geometry of the boundaries, forming concentric convection rolls illustrated in figure 1.11(b). Interestingly, hexagonal cells have been observed in buoyancy-driven flows of non-Boussinesq fluids ([Bodenschatz et al., 2000](#); [Hoard, Robertson, & Acrivos, 1970](#)). In this thesis, we consider the RBP setup (and RBC in chapter 4) with rigid-rigid boundary conditions, bearing critical Rayleigh number of  $Ra_c = 1708$ . Notably, the corresponding critical wavelength is  $q_c = 3.12/d$  (or  $\lambda_c \approx 2d$ ), suggesting that distance separating the plates,  $d$ , dictates the length of a single roll,  $l_{roll} = \lambda_c/2 \approx d$ .

As mentioned earlier, stationary ISRs near  $q_c$  emerge just above  $Ra_c$ , based on weakly nonlinear stability analysis. ([Eckhaus, 1965](#); [Schlüter et al., 1965](#)). However, this prediction contradicted by

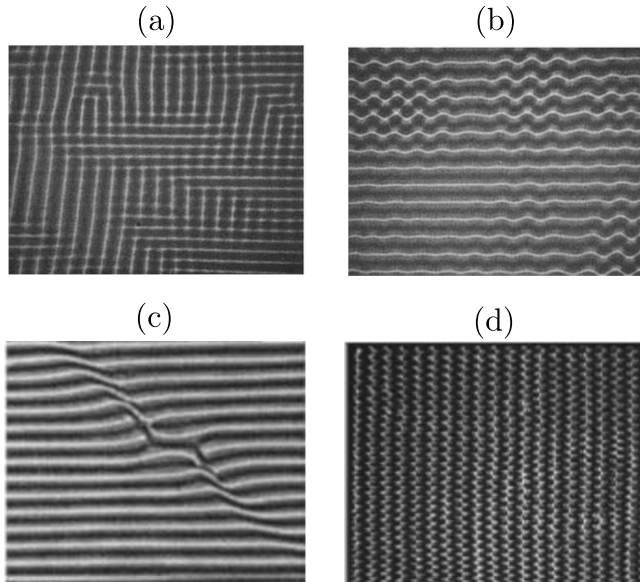


Figure 1.13: ISRs experiencing (a) cross-roll instability at  $Ra = 3000, Pr = 100$  and (b) zig-zag instability at  $Ra = 3600, Pr = 100$  ([Busse & Whitehead, 1971](#)). (c) Skew-varicosed instability at  $Ra = 5568, Pr = 1$  ([Plapp, 1997](#)), and (d) oscillatory instability at  $Ra = 10384, Pr = 1$  ([Cakmur et al., 1997a](#)).

the emergence of time-dependent oscillatory ISRs in experiments ([Rossby, 1969](#); [Willis & Deardorff, 1970](#)) at  $Ra = 9200$  (or roughly five times  $Ra_c$ ), where weakly nonlinear stability analysis becomes inapplicable far from threshold. To address this, a secondary stability analysis was employed to study the stability of ISRs further from  $Ra_c$  ([Busse, 1972](#)). One of the key results from this analysis is the Busse balloon, which describes the stability boundaries of ISRs as a function of  $Ra$  and  $Pr$ , and roll wavenumber,  $\alpha$ , shown figure 1.12 ([Busse, 1978](#)). The boundaries of the Busse balloon are described by a range of secondary instabilities, each arising from different physical mechanisms ([Busse, 1978](#)). At large Prandtl numbers,  $Pr = O(10^2)$ , the zig-zag (ZZ) and cross-roll (CR) instabilities delimits the balloon for small and large roll wavenumbers. The zig-zag instabilities cause zig-zag undulations while the CR instabilities generates rolls orthogonal to the underlying ISR structure, effectively increasing or decreasing the roll wavenumber respectively ([Busse & Whitehead, 1971](#)). Examples of these instabilities at  $Pr = 100$  are illustrated in figure 1.13(a,b).

At moderate Prandtl numbers,  $Pr = O(1)$ , the Busse balloon is bounded by the skewed varicosed (SV) for high roll wavenumbers and the oscillatory (OS) instability at large  $Ra$ . The skewed-varicosed (SV) instability leads to roll-pinch where pinched rolls merged into a single roll, reducing roll wavenumber while the oscillatory instability leads to the onset of an oscillatory ISRs. Examples of the respective instabilities at  $Pr = 1$  are shown in figure 1.13(c,d). At higher wavenumbers, the skewed varicose (SV) instability becomes relevant at intermediate Prandtl numbers, characterised by roll pinching and merging that effectively reduces the roll wavenumber. Finally, the Eckhaus instability (not shown), related to the symmetry of the system, appears close to the  $Ra_c$ , leading a disturbance parallel to the underlying rolls which either creates or destroy rolls such that the resultant roll wavenumber adheres to the stability boundaries ([Lowe & Gollub, 1985](#)). Near  $Pr = 1$ , the Eckhaus instability coincides with the crossroll instability (figure 6 from [Bodenschatz et al. \(2000\)](#),

adapted from [Plapp \(1997\)](#).)

In this thesis, we focus on fluids with  $Pr = 1$ , where secondary instabilities such as skewed-varicose, Eckhaus and cross-roll instabilities typically arise. While the stability boundaries of the Busse balloon have been experimentally verified ([Busse & Whitehead, 1971](#); [Croquette, 1989a](#); [Plapp, 1997](#)), accurately predicting the wavenumber of ideal straight rolls (ISRs) remain difficult due to hysteresis and the existence of multiple stable ISRs of different roll wavenumbers. As  $Ra$  continuously increases, ISRs with wavenumbers outside the Busse Balloon undergo the secondary instabilities (described above) that drive their wavenumbers back to the stable boundaries. The hysteretic behaviour highlights that the roll wavenumber of the ISRs is strongly dependent on the system's history ([Bodenschatz et al., 2000](#)).

It is worth noting that the ISRs are the exception rather than the rule in RBC ([Croquette, 1989b](#)). A range of non-ISR states, such as squares, travelling or stationary target patterns, giant rotating spirals, and oscillatory convection, have been observed over the years ([Borońska & Tuckerman, 2010a, 2010b](#); [Croquette, 1989a](#); [Hof, Lucas, & Mullin, 1999](#); [Le Gal, Pocheau, & Croquette, 1985](#); [Plapp, 1997](#); [Rüdiger & Feudel, 2000](#)). For example, [Hof et al. \(1999\)](#) identified eight stationary and two oscillatory state in cylindrical RBC with small aspect ratios at the same Rayleigh number. These results were later verified in numerical simulations and bifurcation analysis, revealing up to twelve stable branches near the onset ( $Ra \leq 2500$ ) and the potential for hundreds more as  $Ra$  increases ([Borońska & Tuckerman, 2010a, 2010b](#); [Ma, Sun, & Yin, 2006](#)).

In larger domains ( $\Gamma \geq 28$ ), giant rotating spirals were found and have been investigated ([Plapp & Bodenschatz, 1996](#); [Plapp, Egolf, Bodenschatz, & Pesch, 1998](#)). Experimental and numerical studies of RBC with varying sidewall boundary conditions (i.e. thermally insulating, conducting an no-slip) ([Bouillé, Dallas, & Farrell, 2022](#); [M. Paul, Chiam, Cross, Fischer, & Greenside, 2003](#); [Siggers, 2003](#); [Tuckerman & Barkley, 1988](#)), non-Boussinesq convection ([Bodenschatz et al., 1992](#)), and rotational effects ([Hu, Ecke, & Ahlers, 1997](#)) were investigated, where multiple states were also reported. In inclined RBC, [Reetz and Schneider \(2020\)](#); [Reetz, Subramanian, and Schneider \(2020\)](#) identified up to sixteen stable and unstable invariant states, along with heteroclinic orbits connecting them. These findings indicate that RBC support a rich variety of coexisting stables states beyond ISRs, resulting to a system with multiple stable states above the critical Rayleigh number. To complicate matters further, RBC also exhibits spatiotemporal chaotic states.

In the late 1990s, convection rolls exhibiting spatio-temporal chaotic behaviour known as spiral defect chaos (SDC) were observed within the same stability boundaries where ISRs were expected ([Ahlers, n.d.](#); [Cakmur et al., 1997a](#); [Chiam, Paul, Cross, & Greenside, 2003](#); [Decker, Pesch, & Weber, 1994](#); [Egolf, Melnikov, & Bodenschatz, 1998](#); [Egolf, Melnikov, Pesch, & Ecke, 2000](#); [Hu, Ecke, & Ahlers, 1993, 1995](#); [Morris, Bodenschatz, Cannell, & Ahlers, 1993, 1996](#); [Vitral et al., 2020](#)). Notably, ISRs emerge with carefully prepared initial conditions while uncontrolled initial conditions lead to SDC. It is now well established that SDC exists as intrinsic attractor of RBC, independent of sidewall conditions [Morris et al. \(1996\)](#), forming a bistable system with ISRs ([Cakmur et al., 1997a](#)) across a range of  $Ra$  at  $Pr = 1$  illustrated in figure 1.14. However, this bistability appears to be Prandtl number dependent. At  $Pr = 4$ , the SDC appears to be transient decaying towards ISRs over long

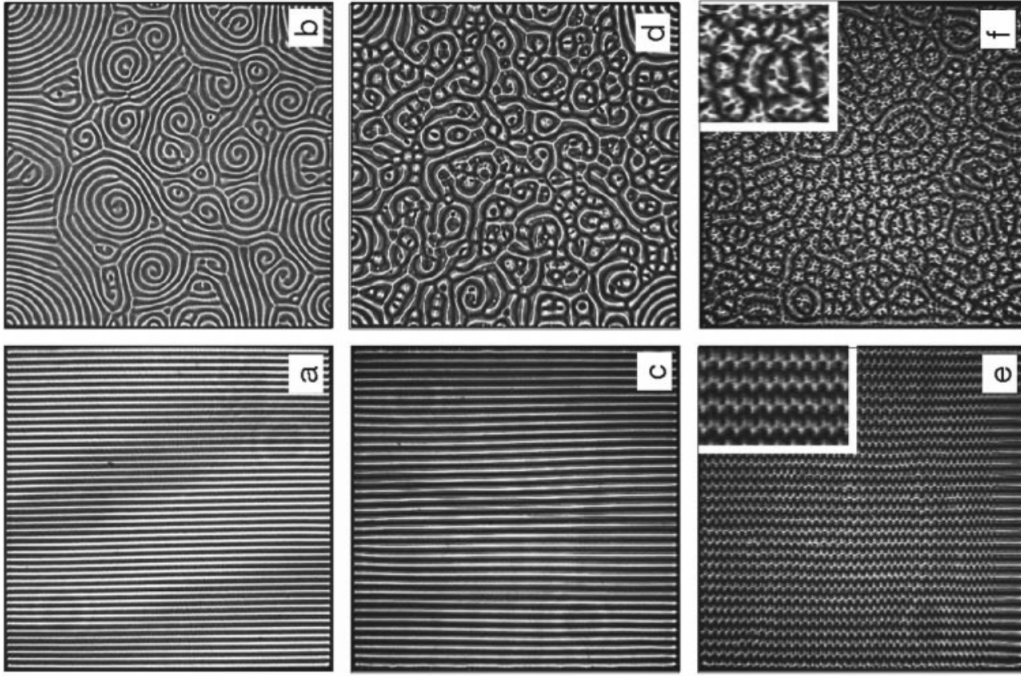


Figure 1.14: The coexistence of spiral defect chaos (SDC, top row) and ideal straight rolls (ISRs, bottom row) at (a,b)  $Ra = 3279$ , (c,d)  $Ra = 6832$  and (e,f)  $Ra = 10384$ . The domain size is  $\Gamma = 50$  and  $Pr = 1$ , adapted from [Cakmur et al. \(1997a\)](#).

periods ([Bajaj, Cannell, & Ahlers, 1997](#)). SDC has also been replicated in numerical simulations using two-dimensional Swift-Hohenberg equations ([Karimi, Huang, & Paul, 2011](#); [Schmitz, Pesch, & Zimmermann, 2002](#); [Swift & Hohenberg, 1977](#); [H. Xi & Gunton, 1995](#); [H.-w. Xi, Gunton, & Viñals, 1993](#)). The critical Rayleigh number for the onset of SDC,  $Ra_s$ , depends on the domain's aspect ratio, and Prandtl number ([Bajaj et al., 1997](#); [Bodenschatz et al., 2000](#); [Cakmur, Egolf, Plapp, & Bodenschatz, 1997b](#); [Hu et al., 1995](#)). SDC has been primarily reported in large aspect ratio domains ( $\Gamma \gtrsim 20$ ), suggesting a minimal domain size for SDC to occur ([Bodenschatz et al., 2000](#)). This is consistent with the leading Lyapunov exponents of SDC which becomes smaller with decreasing  $\Gamma$  ([Egolf et al., 2000](#); [M. R. Paul, Einarsson, Fischer, & Cross, 2007](#)). To better characterise SDC, several studies have investigated its spatial-temporal properties, such as the averaged roll-curvature [Hu et al. \(1995\)](#), probability distribution of spirals [Ecke, Hu, Mainieri, and Ahlers \(1995\)](#); [Liu and Ahlers \(1996\)](#) and correlation length-/time-scales ([Cakmur et al., 1997b](#); [Morris et al., 1993, 1996](#)). Specifically, the correlation length-scales were found to grow exponentially with ([Cakmur et al., 1997b](#); [Morris et al., 1993, 1996](#)), suggesting that transition from ISRs to SDC is related to phase transitions. Similar ‘SDC-lied’ has been observed in other pattern-formation systems, including rotating RBC [Hu et al. \(1997\)](#), dielectric barrier discharge [Dong, Liu, Liu, He, and Fan \(2005\)](#) and advection diffusion reaction systems [Affan and Friedrich \(2014\)](#).

## 1.4 Rayleigh-Bénard Poiseuille (RBP) flows

This section describes the developments of Rayleigh-Bénard Poiseuille (RBP) flows, integrating key findings from both plane Poiseuille flow (PPF) and Rayleigh-Bénard convection (RBC) systems

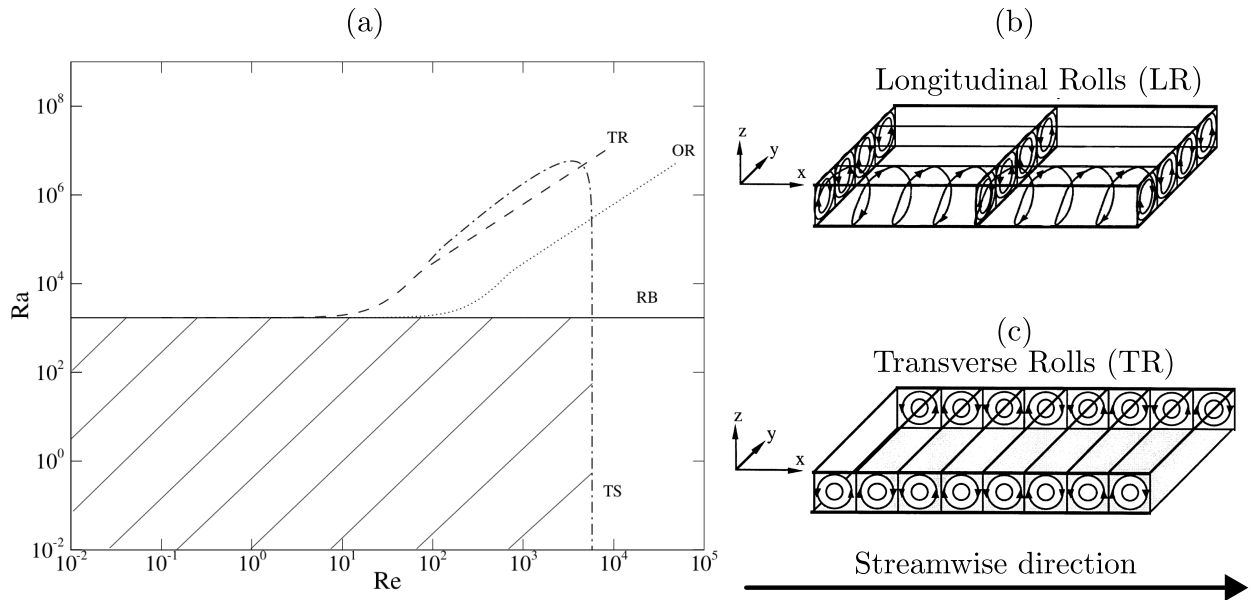


Figure 1.15: (a) Neutral stability curves of longitudinal rolls (LR), oblique rolls (OR), transverse rolls (TR) and Tollmien-Schlichting (TS) waves, adapted from [John Soundar Jerome et al. \(2012\)](#). The shaded area refers to damped perturbations. Sketch of (b) longitudinal and (c) transverse rolls, adapted from [Kelly \(1994\)](#).

discussed in §1.2 and §1.3 respectively. The neutral stability curves in the Rayleigh-Bénard Poiseuille (RBP) comprising of both plane Poisueuille flow (PPF) and Rayleigh-Bénard convection (RBC) systems, are bounded by the onset of Tollmien-Schlichting waves at  $Re_c = 5772.22$  ([Orszag, 1971](#)), and by the onset of convection rolls at  $Ra_c = 1708$  ([Pellew & Southwell, 1940](#)), respectively. In RBP systems, the imposed mean Poiseuille flow in the RBP system breaks the rotational symmetry of the convection rolls, categorising them based on their orientation to the mean flow direction, namely: longitudinal, transverse and oblique rolls. These primary instabilities were first investigated by [Gage and Reid \(1968\)](#) in an infinitely extended layer. For longitudinal rolls, the linearised system reduces to the classical RBC problem. Thus, the critical Rayleigh number remains unchanged at  $Ra_{\parallel} = Ra_c = 1708.8$  with a critical wavenumber,  $\alpha_{\parallel} = \alpha_c = 3.13$ , independent of Reynolds number and Prandtl number ([Kelly, 1994](#); [Pellew & Southwell, 1940](#)). In contrast, the critical Rayleigh number for the onset of transverse rolls increases with  $Re$ , and is also dependent on  $Pr$  ([Gage & Reid, 1968](#); [Müller, Lücke, & Kamps, 1992](#); [Nicolas, Mojtabi, & Platten, 1997](#)). The critical Rayleigh number for the onset of obliqued rolls can derived using by applying a Squire transformation ([Squire, 1933](#)) to transverse roll system. For a given  $Ra$ , the corresponding critical  $Re$  for the onset of oblique rolls is higher than that for transverse rolls ([Gage & Reid, 1968](#)). The neutral stability curves for the three different rolls are illustrated in figure 1.15.

Experimental studies in channels with large transverse aspect ratios (i.e. span-to-depth) showed the onset of longitudinal rolls ([Akiyama, Hwang, & Cheng, 1971](#); [Fukui, Nakajima, & Ueda, 1983](#); [Ostrach & Kamotani, 1975](#)), while transverse rolls are more prevalent in narrower channels ([Luijkh, Platten, & Legros, 1981](#); [Ouazzani, Caltagirone, Meyer, & Mojtabi, 1989](#); [Ouazzani, Platten, & Mojtabi, 1990](#)). Linear stability analysis of longitudinal rolls for finite channels confirms that  $Ra_{\parallel}$  remains fairly independent for transverse aspect ratios greater than five, and increases quickly below that. Hence,

for small  $Re$ , critical Rayleigh number of transverse rolls is smaller than that of longitudinal rolls,  $Ra_{\perp} < Ra_{\parallel}$ , giving rise to transverse rolls (Nicolas, Luijckx, & Platten, 2000). However, laminar Poiseuille flow where observed in the same parameter space where transverse rolls were expected from linear stability analysis Ouazzani et al. (1989). This discrepancy was resolved by Müller et al. (1992), who showed that transverse rolls may be convectively or absolutely unstable, with the transition boundary corroborating with experimental data. Later, Carrière and Monkewitz (1999) showed that demonstrated that longitudinal rolls are always convectively unstable. Nonmodal stability analysis of subcritical RBP by John Soundar Jerome et al. (2012) revealed that the optimal transient growth is primarily dominated by streamwise rollers similar to those of PPF (Reddy & Henningson, 1993), with a spanwise wavenumber of  $\beta_{opt} \approx 2.05$ . The maximum amplification factor,  $G_{max}$  increases modestly with  $Ra$ , and the critical wavenumber approaches  $\alpha_{\parallel}$ , indicative of longitudinal rolls.

For  $Re > 0$  in infinite domains, the longitudinal rolls emerge as the dominant primary instability (Gage & Reid, 1968), and their secondary stability was analysed by Clever and Busse (1991). They identified a time-dependent, wavy instability near  $Re \sim 100$ , giving rise to tertiary solutions in the form of wavy rolls. These wavy rolls have been observed experimentally and were found to be convectively unstable (Nicolas, Xin, & Zoueidi, 2010; Pabiou, Mergui, & Bénard, 2005; Pabiou, Nicolas, Xin, & Mergui, 2003). Clever and Busse (1991) also hypothesised that the wavy rolls are less efficient at transporting heating than longitudinal rolls for the same  $Ra$ , which was later confirmed numerically by Nicolas, Zoueidi, and Xin (2012). The influence of finite transverse aspect ratios on the onset of wavy rolls have also been studied (Nicolas et al., 2010; Xin, Nicolas, & Quéré, 2006), where the critical  $Ra$  was found to be approximately 1.5 times higher than in infinite domains Clever and Busse (1991). Furthermore, the effect of external excitation has been explored, showing that increased excitation amplitude can reduce the development length required for the formation of wavy roll (Nicolas et al., 2010, 2012). In the turbulent regime, shear driven turbulence has been shown to enhance heat transport in RBP flows (Pirozzoli, Bernardini, Verzicco, & Orlandi, 2017; Scagliarini, Einarsson, Gylfason, & Toschi, 2015; Scagliarini, Gylfason, & Toschi, 2014). Extensions of the RBP configuration, such as flows over wavy walls or with sinusoidal thermal forcing have been investigated, potentially offering a reduction in drag and enhancing heat transport (Hossain, Floryan, & Floryan, 2012; Hossain & Floryan, 2016, 2020). For a comprehensive overview of RBP flows, the reader is referred to the reviews by Kelly (1994) and Nicolas (2002).

## 1.5 Thesis Outline

In this thesis, I focus on the transitional behaviour of fluid flow in Rayleigh-Bénard Poiseuille systems by conducting direct numerical simulations and linear stability analysis. Notably, the onset of instabilities does not necessarily lead to turbulence and may give rise to flow regimes that are neither fully laminar nor fully turbulent. For clarity, we refer to these flow regimes collectively as the transitional regime.

While significant progress has been made in understanding the transition process of Rayleigh-Bénard convection and plane Poiseuille flows separately, their combined effects remains largely

unexplored. For instance, do convection rolls promote the transition to shear driven turbulence? And conversely, how does shear affect the bistable dynamics between ideal straight rolls (ISRs) and spiral defect chaos (SDC)? These questions are explore in §??.

Although the co-existence of ISRs and SDC as bistable states in Rayleigh-Bénard convection is well established, the existence of multiple states raises further questions about the notion of bistability. In §??, we investigate the state-space structure underlying ISRs and SDC, identifying several stable invariant solutions referred to as *elementary* states that underpin the pattern formation of SDC.

The thesis is structured into the follows:

1. §1 provides the introduction and a review of relevant literature.
2. §?? presents the numerical methods, including the spectral/*hp* element method, algorithms for solving the Navier-Stokes equations, linear stability analysis and edge tracking.
3. §?? introduces the  $Ra - Re$  phase space of RBP flows, with a particular focus on the role of longitudinal rolls in sustaining turbulence. We introduce the *thermally-assisted sustaining process* - an alternative route towards turbulence via linearly unstable longitudinal rolls
4. §?? explores the organisation of the state space of spiral defect chaos and ideal straight rolls  $Ra = 2903$ , accompanied by *elementary* states, edge states and highlight some pathways towards SDC
5. Finally, §?? concludes this thesis and suggests possible avenues of future research.



# Appendix A

## Appendices

### A.1 Simulation parameters for $Ra$ - $Re$ sweep

The spectral/ $hp$  quadrilateral element width, heights and polynomial order are kept constant for all simulations,  $(\Delta x, \Delta y|_{y=\pm h}, \Delta y|_{y=0}, P) = (0.1\pi, 0.0549, 0.367, 4)$ . To resolve the high gradients, the quadrilateral element heights are bunched near the wall,  $\Delta y|_{y=\pm h}$ , and expanded in the channel center,  $\Delta y|_{y=0}$ . The basis type employed here consists of the modified Jacobi polynomials, known as the *modified* basis (see §??). Table A.1 describes the number of Fourier expansions,  $N_z$ , and temporal resolution of 52 numerical experiments at  $Re = 0, 0.1, 1, 10, 100, 500, 750, 1000, 1050, 2000$ , and  $Ra = 0, 2000, 3000, 5000, 8000, 10000$  with  $Pr = 1$  and a large aspect ratio,  $\Gamma = 4\pi$ . The initial conditions of all numerical experiments were sampled from a statistically stationary solution based on the time history of the Nusselt number and shear. The laminar solution obtained for  $Ra = 0$ ,  $Re \leq 1000$  has been omitted in table A.1.

### A.2 First- and second-order statistics of the buoyancy- and shear-driven regime

#### A.2.1 Buoyancy-driven regime

We present the first- and second-order statistics of the buoyancy-dominated regime (shaded in red), consisting of the (1) SDC & ISRs, and (2) ISRs states in figure A.1, illustrating its temporal and plane-averaged streamwise velocity,  $\langle w \rangle_{x,z,t}$ , temperature,  $\langle \theta \rangle_{x,z,t}$ , fluctuating wall-normal velocity squared normalised by thermal velocity scale,  $\langle \tilde{v}\tilde{v} \rangle_{x,z,t}/u_\kappa^2$ , fluctuating temperature squared,  $\langle \tilde{\theta}\tilde{\theta} \rangle_{x,z,t}$  and fluctuating span- and streamwise velocities squared normalised by thermal velocity scale,  $\langle \tilde{u}\tilde{u} + \tilde{w}\tilde{w} \rangle_{x,z,t}/u_\kappa^2$ . We note that the fluctuating components are defined about a temporal-planar averaged quantity, i.e  $\tilde{\mathbf{u}} = \mathbf{u} - \langle \mathbf{u} \rangle_{x,z,t}$ . The mean temperature profiles (figure A.1(b)), and the fluctuating span- and streamwise velocities (figure A.1(f)) are visually similar for the same  $Ra$ , and are nearly independent of  $Re$ . However, we observe the dependence on  $Re$  at  $Ra = 3000$  in the fluctuating temperature squared (figure A.1(d)), and fluctuating wall-normal velocities (figure A.1(c)), likely due to variations in convection structures, particularly in the convection roll wavenumbers. A detailed

Ra	Re	$N_z$	$dt$	$T$	$\frac{d}{\kappa}$
0	1050	64	0.1	8000	-
0	2000	128	0.02	3000	-
2000	0	64	0.05	50	25
2000	0.1	64	0.005	5	25
2000	1	64	0.01	50	25
2000	10	64	0.05	50	2.5
2000	100	64	0.1	50	0.25
2000	500	64	0.1	50	0.05
2000	750	64	0.1	50	0.033
2000	1000	64	0.1	50	0.025
2000	1050	64	0.1	8000	3.81
2000	2000	128	0.02	2800	0.75
3000	0	64	0.05	3000	1500
3000	0.1	64	0.005	300	1500
3000	1	64	0.05	100	50
3000	10	64	0.05	50	2.5
3000	100	64	0.1	10000	50
3000	500	64	0.1	50	0.05
3000	750	64	0.1	50	0.033
3000	1000	64	0.1	50	0.025
3000	1050	64	0.1	8000	3.81
3000	2000	128	0.02	2800	0.75
5000	0	64	0.005	1200	600
5000	0.1	64	0.001	800	4000
5000	1	64	0.01	2500	1250
5000	10	64	0.05	500	25
5000	100	64	0.1	1000	5
5000	500	64	0.05	8000	8
5000	750	64	0.05	8000	5.33
5000	1000	64	0.02	8000	4
5000	1050	64	0.02	8000	3.81
5000	2000	128	0.02	2800	0.75
8000	0	64	0.0025	600	300
8000	0.1	64	0.0005	600	3000
8000	1	64	0.005	600	300
8000	10	64	0.05	500	25
8000	100	64	0.1	5000	25
8000	500	64	0.05	10000	10
8000	750	64	0.05	8000	5.33
8000	1000	64	0.02	8000	4
8000	1050	64	0.02	8000	3.81
8000	2000	128	0.02	2800	0.75
10000	0	64	0.0025	1000	500
10000	0.1	64	0.00025	800	4000
10000	1	64	0.0025	600	300
10000	10	64	0.05	12000	600
10000	100	64	0.1	8000	40
10000	500	64	0.05	8000	8
10000	750	64	0.05	8000	5.33
10000	1000	64	0.02	8000	4
10000	1050	64	0.02	8000	3.81
10000	2000	128	0.02	2800	0.75

Table A.1: The summary of the spatial and temporal resolution for a given  $Re$ ,  $Ra$ .  $N_z$  denotes the number of Fourier expansions in the  $z$ -direction.  $dt, T, d/\kappa$  denotes the timestep, final time and the final time scaled by the thermal timescale.

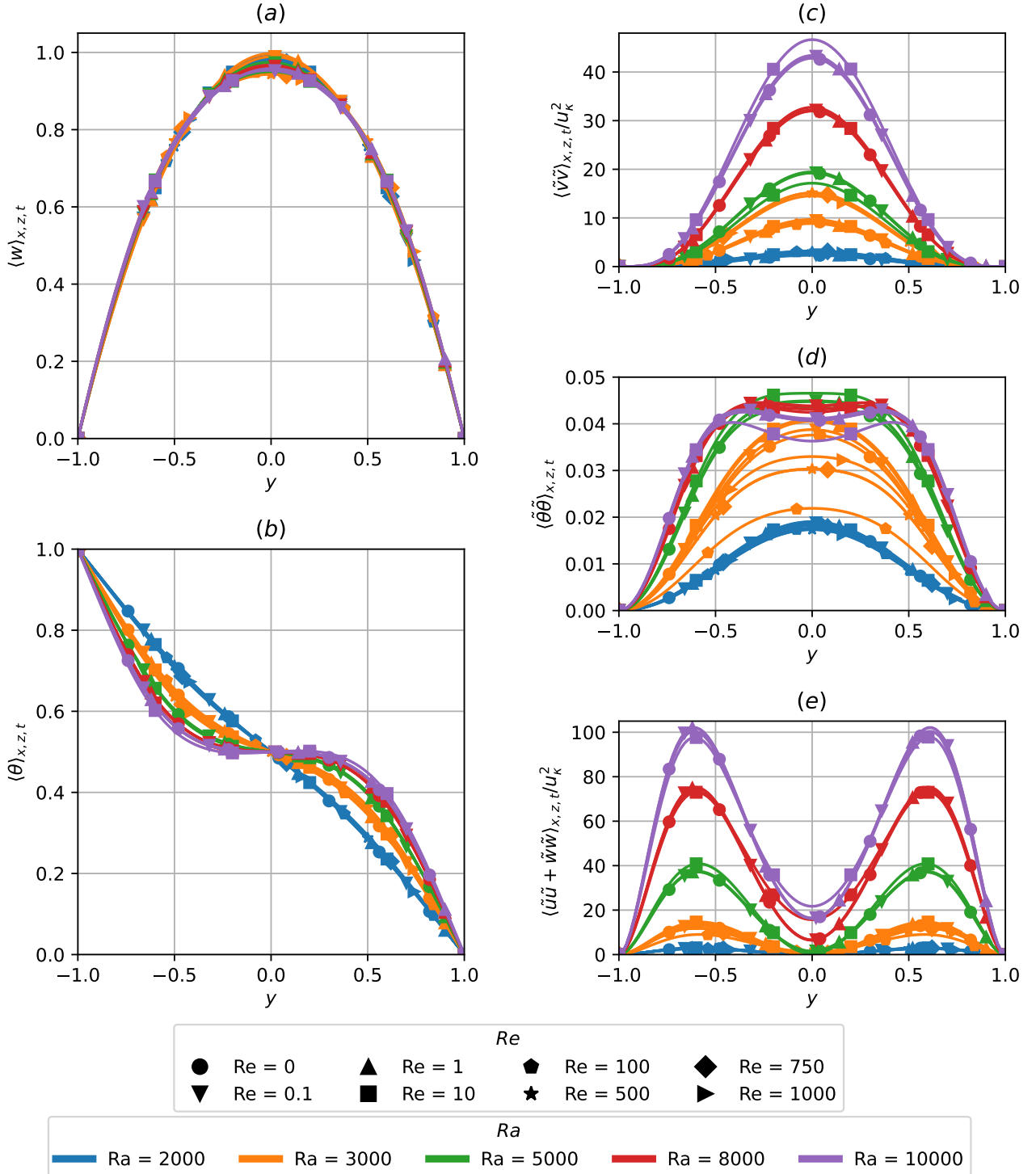


Figure A.1: The wall-normal distribution of temporal and plane- averaged (a) streamwise velocity, (b) temperature, (c) fluctuating wall-normal velocity squared normalised by thermal velocity scale, (d) fluctuating temperature squared and (e) fluctuating span- and streamwise velocities squared normalised by thermal velocity scale of buoyancy-driven regime shaded in red in figure ??.

analysis of how the statistical properties vary with roll wavenumber is beyond the scope of this work. We propose that the underlying flow structure, consisting of convection rolls, describes the buoyancy-driven regime, shaded in red in figure ???. In this regime, the strength of the convection is primarily controlled by  $Ra$ , akin to RBC, and remains independent of  $Re$ .

### A.2.2 Shear-driven regime

As  $Re$  falls within the range of  $1050 \leq Re \leq 2000$ , shear-driven turbulence dominates, where the impact of  $Ra$  on the first- and second-order statistics is weakly dependent on  $Ra$  in figure A.2. Figure A.2 describes the temporal and plane-averaged streamwise velocity,  $\langle w \rangle_{x,z,t}$ , temperature,  $\langle \theta \rangle_{x,z,t}$ , fluctuating streamwise velocity squared,  $\langle \tilde{w}\tilde{w} \rangle_{x,z,t}$ , fluctuating wall-normal velocity squared,  $\langle \tilde{v}\tilde{v} \rangle_{x,z,t}$ , fluctuating spanwise velocities squared,  $\langle \tilde{u}\tilde{u} \rangle_{x,z,t}$ , fluctuating Reynolds stresses  $\langle \tilde{v}\tilde{w} \rangle_{x,z,t}$ , and fluctuating temperature squared,  $\langle \tilde{\theta}\tilde{\theta} \rangle_{x,z,t}$  at  $Re = 2000, 1050$  for  $Ra \in [0, 10000]$ . The flow structures appear as uniform, featureless turbulence (Tuckerman et al., 2014) at  $Re = 2000$ , independent of  $Ra$ . The spacetime figure of near-wall ( $y^+ = 15$ ), wall-normal and spanwise perturbation kinetic energy,  $\mathcal{E}_{u'+v'}$ , at  $Re = 2000$ ,  $t \in [0, 2800]$ , illustrating spatially uniform featureless turbulence, visually distinguishable with  $Ra \in [0, 10000]$ , corroborating with their  $Ra$ -independent first- and second-order statistics in figure A.2. In other words, the dominant physical mechanism is shear-driven turbulence at  $Re = 2000$ , independent of  $Ra$ .

As  $Re$  approaches  $Re = 1050$ , the midplane temperature in figure ?? shows regions of spatially localised structures, indicating the presence of turbulent-laminar bands, described in figure ?? and ?? later. The mean streamwise velocity and temperature gradients at both ends of the wall, and second-order statistics, are enhanced slightly from  $Ra = 0$  to  $Ra = 10000$ . This enhancement could be due to the coexistence of longitudinal rolls with turbulent bands at  $Ra = 10000$ , discussed in §???. Notably, we have also included the statistics for a subcritical case ( $Ra < Ra_{\parallel}$ ) at  $Ra = 1000$ , indicating the presence of subcritical effects as the statistics are slightly enhanced from  $Ra = 0$  to  $Ra = 1000$ , reported by John Soundar Jerome et al. (2012). Nonetheless, there is a distinct change of state between  $Re = 1000$  to  $1050$  (see figure ??), marked by the transition from the longitudinal/intermittent roll regime to shear-driven turbulence at  $Re \geq 1050$ , thus, shaded in blue in figure ??.

## A.3 Growth rates of primary instabilities

Figure A.4 shows the eigenvalues of the primary instabilities as a function of its spanwise wavenumber  $\alpha d$ , leading to the onset of longitudinal rolls at  $Re = 1050$ . The results are obtained using a Chebyshev-collocation method discretised by 51 Chebyshev polynomials (Driscoll, Hale, & Trefethen, 2014). The crosses denote the spanwise wavenumbers admissible within the domain  $\Gamma = \pi/2$ , where  $\alpha d = 4$  corresponds to the dominant eigenmode.

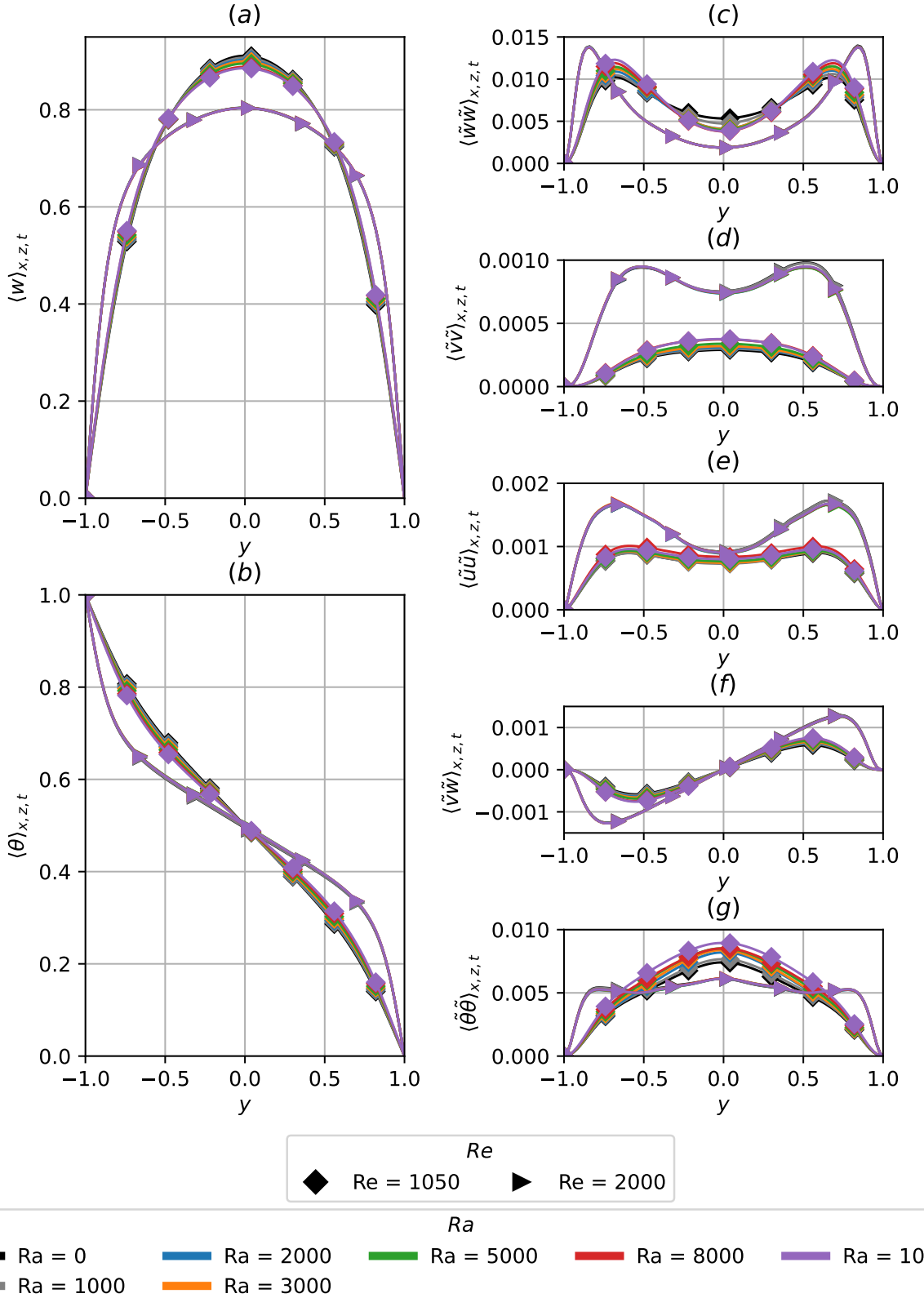


Figure A.2: The wall-normal distribution of temporal and plane- averaged (a) streamwise velocity, (b) temperature, (c) fluctuating streamwise velocity squared, (d) fluctuating wall-normal velocity squared, (e) fluctuating spanwise velocities squared, (f) fluctuating Reynolds stresses and (g) fluctuating temperature squared in the shear-driven regime shaded in blue in figure ??.

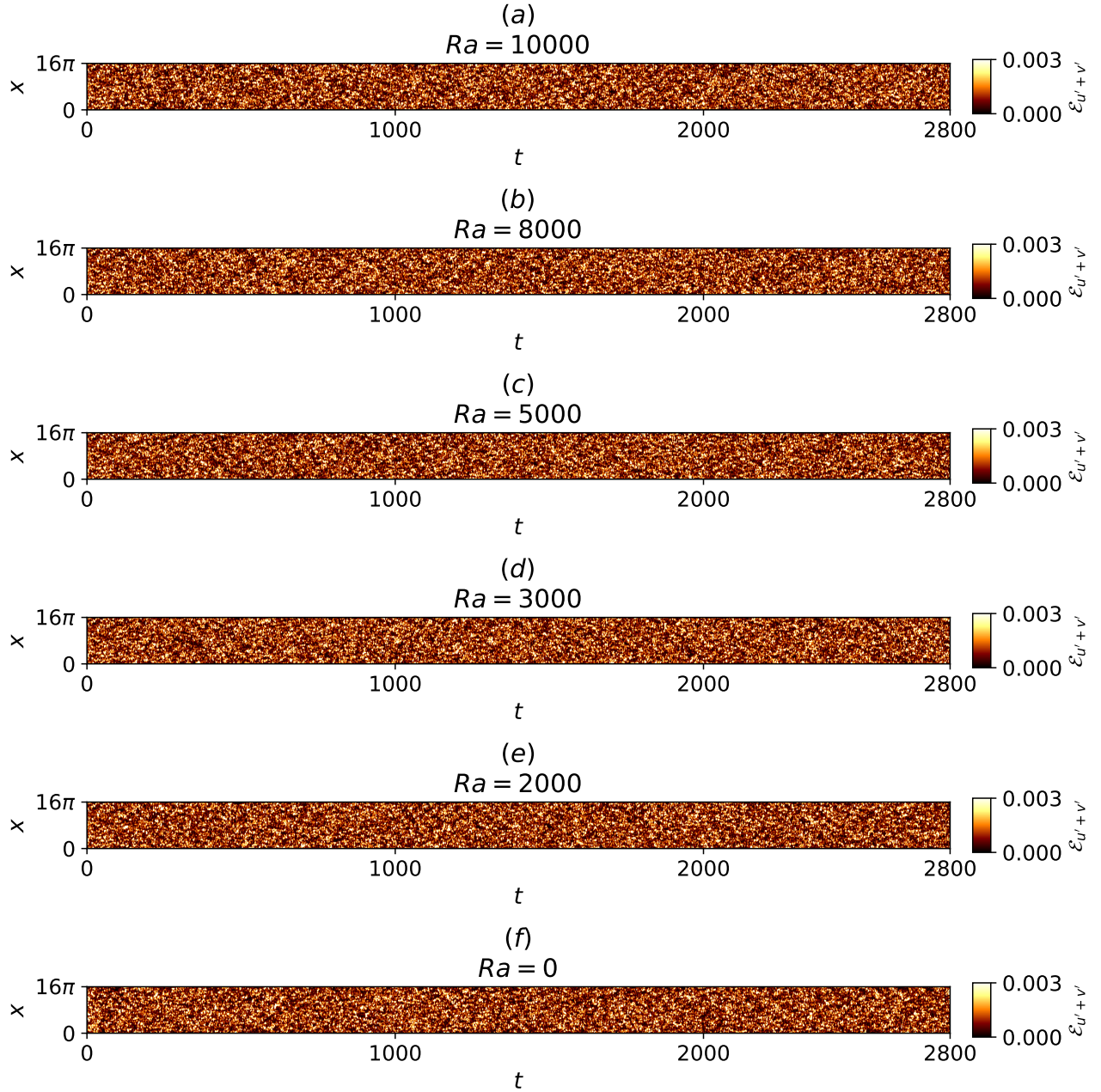


Figure A.3: Spacetime plots of near-wall, wall-normal and spanwise perturbation kinetic energy for  $Re = 2000$ ,  $t \in [0, 2800]$ ,  $\Gamma = 4\pi$  at (a)  $Ra = 10000$ , (b)  $Ra = 8000$ , (c)  $Ra = 5000$ , (d)  $Ra = 3000$ , (e)  $Ra = 2000$ , (f)  $Ra = 0$ .

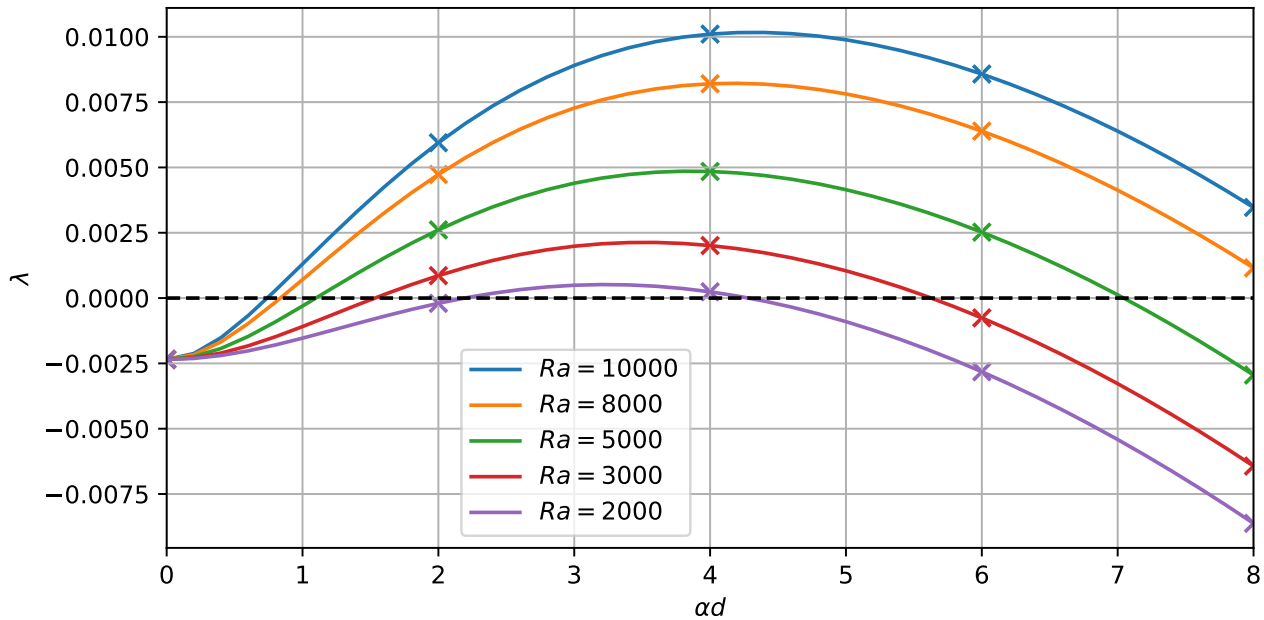


Figure A.4: Growth rates of primary instabilities at  $Ra = 10000, 8000, 5000, 3000, 2000$  leading to the onset of longitudinal rolls against spanwise wavenumber of  $\alpha d$  at  $Re = 1050$ .

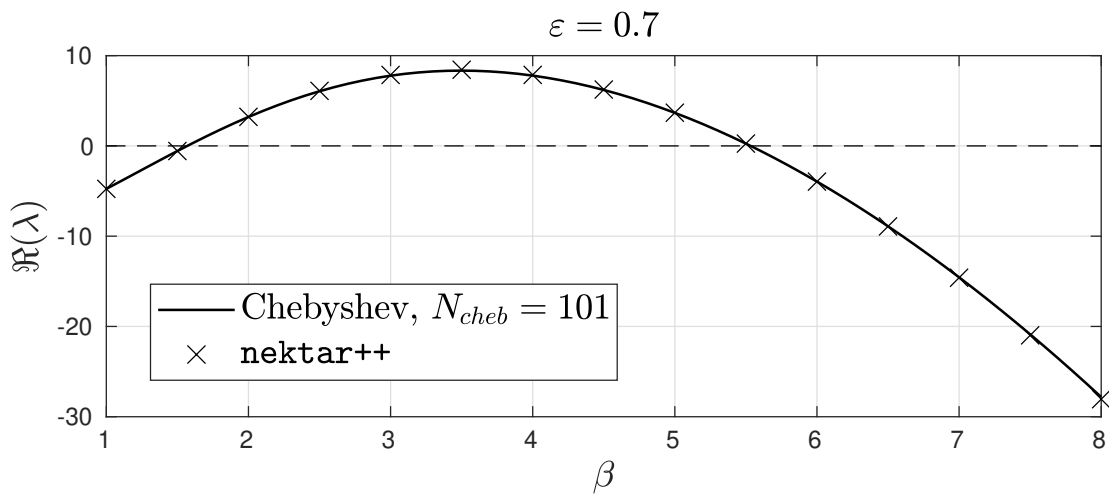


Figure A.5: Eigenvalues of primary instabilities of RBC at  $\varepsilon = 0.7$  computed in Nektar++ compared against a Chebyshev-collocation method with 101 Chebyshev expansions.

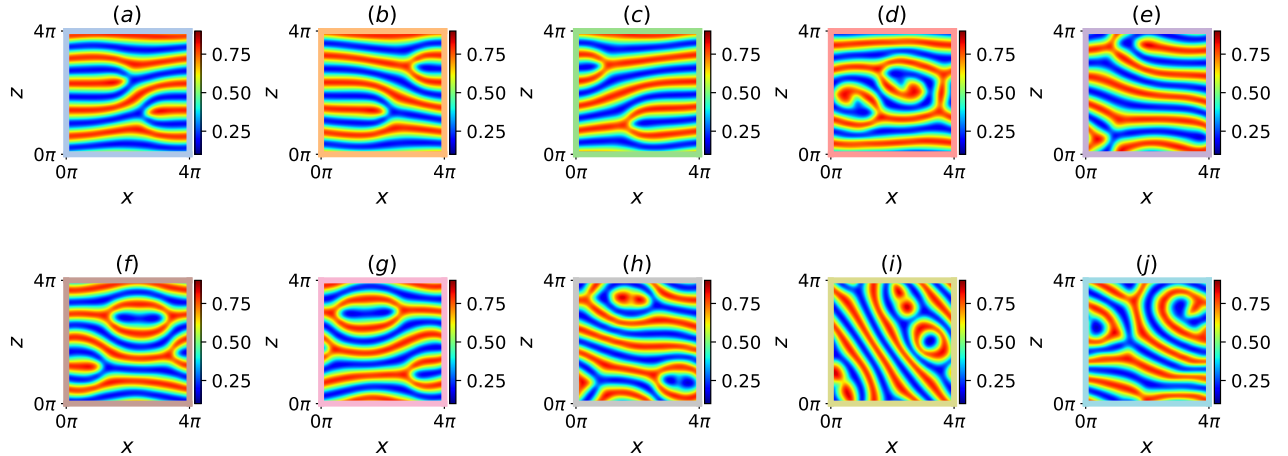


Figure A.6: Temperature snapshots,  $\theta(x, z)|_{y=d/2}$ , of 10 elementary states confined within a minimal domain  $\Gamma = 2\pi$ : (a) steady ‘forked-A’ state, (b) steady ‘forked-B’ state, (c) steady ‘forked-c’ state, (d) steady ‘twin-armed’ state, (e) steady ‘tri-rolls’ state, (f) travelling-wave ‘O-a’ state, (g) travelling-wave ‘O-b’ state, (h) steady ‘keyhole’ state, (i) relative periodic orbit ‘eye’ state, (j) relative periodic orbit ‘S’ state

## A.4 Verification of linear stability analysis

Figure A.5 shows the eigenvalues as a function of spanwise wavenumber  $\beta$  of RBC at  $\varepsilon = 0.7$ . The results are obtained using Nektar++ and compared against a Chebyshev-collocation method discretised by 101 Chebyshev polynomials Driscoll et al. (2014).

## A.5 Other elementary states and ISRs

Figure A.6 presents snapshots of temperature slices  $(\theta(x, z)|_{d/2})$ , depicting ten distinct elementary states. These states are obtained within a minimal domain  $\Gamma = 2\pi$ , consisting of eight stationary states (figures A.6(a-h)) and two travelling-wave states (figures A.6(i,j)). Figure A.7 features a snapshot of fourteen ideal straight rolls (ISRs), and they satisfy rotational symmetry about the  $y$ -axis and mirror symmetries about the  $x$ - and  $z$ -axes due to the horizontal isotropy of the present system. These ISRs represent stable fixed-points in the state space of figures ??, ??, ??, ??.

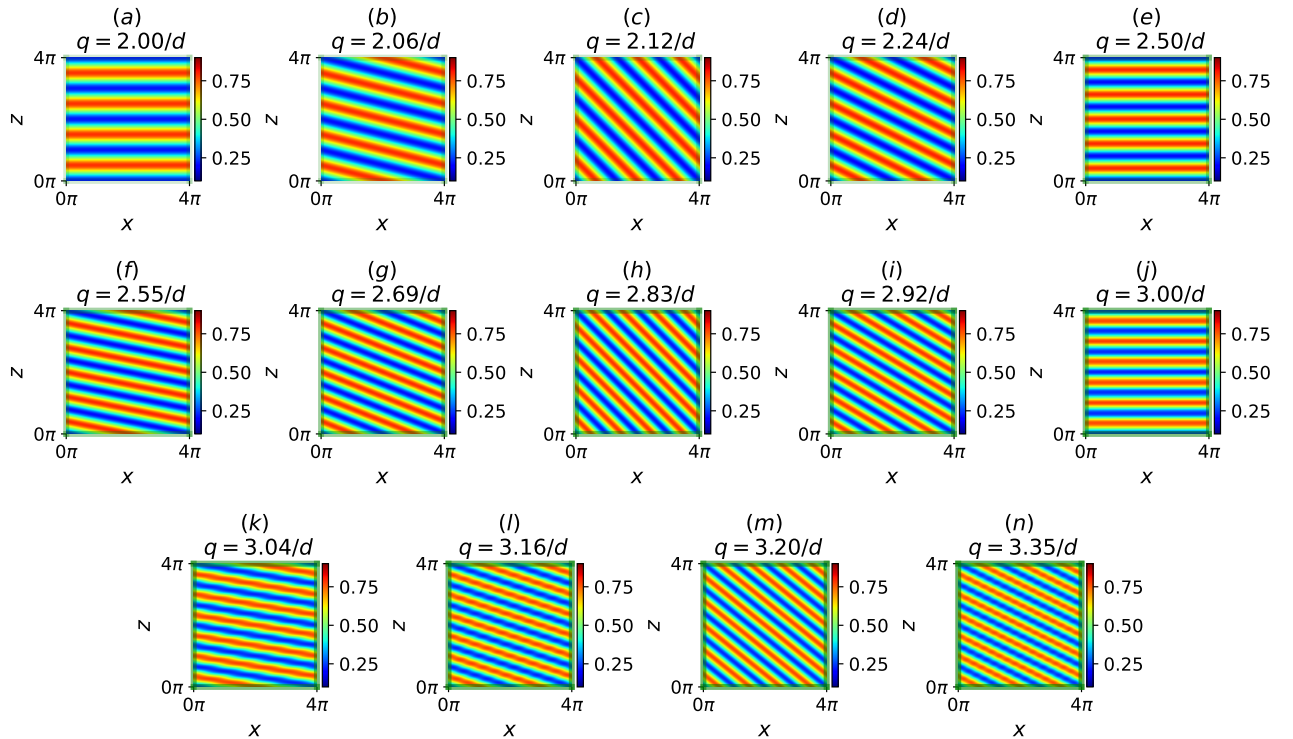


Figure A.7: Temperature snapshots,  $\theta(x, z)|_{y=d/2}$ , of 14 stable ideal straight rolls (ISRs) confined within a minimal domain,  $\Gamma = 6.28$ . Plots (a-n) are ordered in increasing wavenumbers,  $q \in (2/d, 3.35/d)$ .



# References

- Affan, H., & Friedrich, R. (2014, June). Spiral defect chaos in an advection-reaction-diffusion system. *Physical Review E*, 89(6), 062920.
- Ahlers, G. (n.d.). Experiments on spatio-temporal chaos.
- Akiyama, M., Hwang, G.-J., & Cheng, K. (1971). Experiments on the onset of longitudinal vortices in laminar forced convection between horizontal plates.
- Avila, K., Moxey, D., De Lozar, A., Avila, M., Barkley, D., & Hof, B. (2011, July). The Onset of Turbulence in Pipe Flow. *Science*, 333(6039), 192–196. Retrieved 2025-04-01, from <https://www.science.org/doi/10.1126/science.1203223> doi: 10.1126/science.1203223
- Avila, M., Barkley, D., & Hof, B. (2023, January). Transition to Turbulence in Pipe Flow. *Annual Review of Fluid Mechanics*, 55(1), 575–602. Retrieved 2025-04-08, from <https://www.annualreviews.org/doi/10.1146/annurev-fluid-120720-025957> doi: 10.1146/annurev-fluid-120720-025957
- Avila, M., Willis, A. P., & Hof, B. (2010, March). On the transient nature of localized pipe flow turbulence. *Journal of Fluid Mechanics*, 646, 127–136. Retrieved 2025-04-08, from [https://www.cambridge.org/core/product/identifier/S0022112009993296/type/journal\\_article](https://www.cambridge.org/core/product/identifier/S0022112009993296/type/journal_article) doi: 10.1017/S0022112009993296
- Bajaj, K. M. S., Cannell, D. S., & Ahlers, G. (1997, May). Competition between spiral-defect chaos and rolls in Rayleigh-Bénard convection. *Physical Review E*, 55(5), R4869–R4872. Retrieved 2025-03-25, from <https://link.aps.org/doi/10.1103/PhysRevE.55.R4869> doi: 10.1103/PhysRevE.55.R4869
- Barkley, D., & Tuckerman, L. S. (2005, January). Computational Study of Turbulent Laminar Patterns in Couette Flow. *Physical Review Letters*, 94(1), 014502. Retrieved from <https://link.aps.org/doi/10.1103/PhysRevLett.94.014502> (Publisher: American Physical Society) doi: 10.1103/PhysRevLett.94.014502
- Barkley, D., & Tuckerman, L. S. (2007). Mean flow of turbulent-laminar patterns in plane Couette flow. *Journal of Fluid Mechanics*, 576, 109–137. (Publisher: Cambridge University Press)
- Block, M. J. (1956, September). Surface Tension as the Cause of Bénard Cells and Surface Deformation in a Liquid Film. *Nature*, 178(4534), 650–651. Retrieved 2025-04-11, from <https://www.nature.com/articles/178650a0> doi: 10.1038/178650a0
- Bodenschatz, E., Cannell, D. S., De Bruyn, J. R., Ecke, R., Hu, Y.-C., Lerman, K., & Ahlers, G. (1992, December). Experiments on three systems with non-variational aspects. *Physica D: Nonlinear Phenomena*, 61(1-4), 77–93. Retrieved 2025-04-11, from <https://linkinghub.elsevier>

- .com/retrieve/pii/016727899290150L doi: 10.1016/0167-2789(92)90150-L
- Bodenschatz, E., Pesch, W., & Ahlers, G. (2000, January). Recent Developments in Rayleigh-Bénard Convection. *Annual Review of Fluid Mechanics*, 32(1), 709–778. Retrieved 2025-03-25, from <https://www.annualreviews.org/doi/10.1146/annurev.fluid.32.1.709> doi: 10.1146/annurev.fluid.32.1.709
- Borońska, K., & Tuckerman, L. S. (2010a, March). Extreme multiplicity in cylindrical Rayleigh-Bénard convection. II. Bifurcation diagram and symmetry classification. *Physical Review E*, 81(3), 036321. Retrieved 2025-03-25, from <https://link.aps.org/doi/10.1103/PhysRevE.81.036321> doi: 10.1103/PhysRevE.81.036321
- Borońska, K., & Tuckerman, L. S. (2010b, March). Extreme multiplicity in cylindrical Rayleigh-Bénard convection. I. Time dependence and oscillations. *Physical Review E*, 81(3), 036320. Retrieved 2025-03-25, from <https://link.aps.org/doi/10.1103/PhysRevE.81.036320> doi: 10.1103/PhysRevE.81.036320
- Bottin, S., Daviaud, F., Manneville, P., & Dauchot, O. (1998, July). Discontinuous transition to spatiotemporal intermittency in plane Couette flow. *Europhysics Letters (EPL)*, 43(2), 171–176. Retrieved 2025-05-26, from <https://iopscience.iop.org/article/10.1209/epl/i1998-00336-3> doi: 10.1209/epl/i1998-00336-3
- Boullié, N., Dallas, V., & Farrell, P. E. (2022, May). Bifurcation analysis of two-dimensional Rayleigh-Bénard convection using deflation. *Physical Review E*, 105(5), 055106. Retrieved 2025-03-25, from <https://link.aps.org/doi/10.1103/PhysRevE.105.055106> doi: 10.1103/PhysRevE.105.055106
- Busse, F. H. (1972, March). The oscillatory instability of convection rolls in a low Prandtl number fluid. *Journal of Fluid Mechanics*, 52(1), 97–112. Retrieved 2025-03-25, from [https://www.cambridge.org/core/product/identifier/S0022112072002988/type/journal\\_article](https://www.cambridge.org/core/product/identifier/S0022112072002988/type/journal_article) doi: 10.1017/S0022112072002988
- Busse, F. H. (1978, December). Non-linear properties of thermal convection. *Reports on Progress in Physics*, 41(12), 1929–1967. Retrieved 2025-03-25, from <https://iopscience.iop.org/article/10.1088/0034-4885/41/12/003> doi: 10.1088/0034-4885/41/12/003
- Busse, F. H., & Whitehead, J. A. (1971, May). Instabilities of convection rolls in a high Prandtl number fluid. *Journal of Fluid Mechanics*, 47(2), 305–320. Retrieved 2025-04-01, from [https://www.cambridge.org/core/product/identifier/S0022112071001071/type/journal\\_article](https://www.cambridge.org/core/product/identifier/S0022112071001071/type/journal_article) doi: 10.1017/S0022112071001071
- Butler, K. M., & Farrell, B. F. (1992, August). Three-dimensional optimal perturbations in viscous shear flow. *Physics of Fluids A: Fluid Dynamics*, 4(8), 1637–1650. Retrieved 2025-04-06, from <https://pubs.aip.org/pof/article/4/8/1637/402702/Three-dimensional-optimal-perturbations-in-viscous> doi: 10.1063/1.858386
- Bénard, H. (1901). Les tourbillons cellulaires dans une nappe liquide. - Méthodes optiques d'observation et d'enregistrement. *Journal de Physique Théorique et Appliquée*, 10(1), 254–266. Retrieved 2025-03-25, from <http://www.edpsciences.org/10.1051/jphystab:0190100100025400> doi: 10.1051/jphystab:0190100100025400

- Cakmur, R. V., Egolf, D. A., Plapp, B. B., & Bodenschatz, E. (1997a, September). Bistability and Competition of Spatiotemporal Chaotic and Fixed Point Attractors in Rayleigh-Bénard Convection. *Physical Review Letters*, 79(10), 1853–1856. Retrieved 2025-03-25, from <https://link.aps.org/doi/10.1103/PhysRevLett.79.1853> doi: 10.1103/PhysRevLett.79.1853
- Cakmur, R. V., Egolf, D. A., Plapp, B. B., & Bodenschatz, E. (1997b, February). *Transition from Spatiotemporal Chaos to Ideal Straight Rolls in Rayleigh-Bénard Convection*. arXiv. Retrieved 2025-03-25, from <http://arxiv.org/abs/patt-sol/9702003> (arXiv:patt-sol/9702003) doi: 10.48550/arXiv.patt-sol/9702003
- Carrière, P., & Monkewitz, P. A. (1999, April). Convective versus absolute instability in mixed Rayleigh–Bénard–Poiseuille convection. *Journal of Fluid Mechanics*, 384, 243–262. Retrieved 2025-03-25, from [https://www.cambridge.org/core/product/identifier/S0022112098004145/type/journal\\_article](https://www.cambridge.org/core/product/identifier/S0022112098004145/type/journal_article) doi: 10.1017/S0022112098004145
- Chandrasekhar, S. (1968, May). The stability of spiral flow between rotating cylinders. *Philosophical Transactions of the Royal Society of London. Series A, Mathematical and Physical Sciences*, 263(1135), 57–91. Retrieved 2025-03-25, from <https://royalsocietypublishing.org/doi/10.1098/rsta.1968.0006> doi: 10.1098/rsta.1968.0006
- Chiam, K.-H., Paul, M. R., Cross, M. C., & Greenside, H. S. (2003, May). Mean flow and spiral defect chaos in Rayleigh-Bénard convection. *Physical Review E*, 67(5), 056206. Retrieved 2025-04-15, from <https://link.aps.org/doi/10.1103/PhysRevE.67.056206> doi: 10.1103/PhysRevE.67.056206
- Clever, R. M., & Busse, F. H. (1991, August). Instabilities of longitudinal rolls in the presence of Poiseuille flow. *Journal of Fluid Mechanics*, 229(-1), 517. Retrieved 2025-03-25, from [http://www.journals.cambridge.org/abstract\\_S0022112091003142](http://www.journals.cambridge.org/abstract_S0022112091003142) doi: 10.1017/S0022112091003142
- Cloot, A., & Lebon, G. (1984, August). A nonlinear stability analysis of the Bénard–Marangoni problem. *Journal of Fluid Mechanics*, 145(-1), 447. Retrieved 2025-04-13, from [http://www.journals.cambridge.org/abstract\\_S0022112084003013](http://www.journals.cambridge.org/abstract_S0022112084003013) doi: 10.1017/S0022112084003013
- Cossu, C., & Hwang, Y. (2017, March). Self-sustaining processes at all scales in wall-bounded turbulent shear flows. *Philosophical Transactions of the Royal Society A: Mathematical, Physical and Engineering Sciences*, 375(2089), 20160088. Retrieved 2025-10-31, from <https://royalsocietypublishing.org/doi/10.1098/rsta.2016.0088> doi: 10.1098/rsta.2016.0088
- Croquette, V. (1989a, March). Convective pattern dynamics at low Prandtl number: Part I. *Contemporary Physics*, 30(2), 113–133. Retrieved 2025-03-25, from <http://www.tandfonline.com/doi/abs/10.1080/00107518908225511> doi: 10.1080/00107518908225511
- Croquette, V. (1989b, May). Convective pattern dynamics at low Prandtl number: Part II. *Contemporary Physics*, 30(3), 153–171. Retrieved 2025-03-25, from <http://www.tandfonline.com/doi/abs/10.1080/00107518908222594> doi: 10.1080/00107518908222594
- Cvitanović, P., & Gibson, J. F. (2010, December). Geometry of the turbulence in wall-bounded shear

- flows: periodic orbits. *Physica Scripta*, *T142*, 014007. Retrieved 2025-04-23, from <https://iopscience.iop.org/article/10.1088/0031-8949/2010/T142/014007> doi: 10.1088/0031-8949/2010/T142/014007
- Davies, S. J., & White, C. M. (1928, May). An experimental study of the flow of water in pipes of rectangular section. *Proceedings of the Royal Society of London. Series A, Containing Papers of a Mathematical and Physical Character*, *119*(781), 92–107. Retrieved 2025-04-25, from <https://royalsocietypublishing.org/doi/10.1098/rspa.1928.0086> doi: 10.1098/rspa.1928.0086
- Dean, R. B. (1978, June). Reynolds Number Dependence of Skin Friction and Other Bulk Flow Variables in Two-Dimensional Rectangular Duct Flow. *Journal of Fluids Engineering*, *100*(2), 215–223. Retrieved 2025-04-25, from <https://asmedigitalcollection.asme.org/fluidsengineering/article/100/2/215/409704/Reynolds-Number-Dependence-of-Skin-Friction-and> doi: 10.1115/1.3448633
- Decker, W., Pesch, W., & Weber, A. (1994, August). Spiral defect chaos in Rayleigh-Bénard convection. *Physical Review Letters*, *73*(5), 648–651. Retrieved 2025-03-25, from <https://link.aps.org/doi/10.1103/PhysRevLett.73.648> doi: 10.1103/PhysRevLett.73.648
- Del Álamo, J. C., & Jiménez, J. (2006, July). Linear energy amplification in turbulent channels. *Journal of Fluid Mechanics*, *559*, 205. Retrieved 2025-04-25, from [http://www.journals.cambridge.org/abstract\\_S0022112006000607](http://www.journals.cambridge.org/abstract_S0022112006000607) doi: 10.1017/S0022112006000607
- Dong, L., Liu, F., Liu, S., He, Y., & Fan, W. (2005, October). Observation of spiral pattern and spiral defect chaos in dielectric barrier discharge in argon/air at atmospheric pressure. *Physical Review E*, *72*(4), 046215. Retrieved 2025-04-15, from <https://link.aps.org/doi/10.1103/PhysRevE.72.046215> doi: 10.1103/PhysRevE.72.046215
- Driscoll, T. A., Hale, N., & Trefethen, L. N. (2014). Chebfun guide.  
(Publisher: Pafnuty Publications, Oxford)
- Duguet, Y., Schlatter, P., & Henningson, D. S. (2010, May). Formation of turbulent patterns near the onset of transition in plane Couette flow. *Journal of Fluid Mechanics*, *650*, 119–129. Retrieved 2025-03-25, from [https://www.cambridge.org/core/product/identifier/S0022112010000297/type/journal\\_article](https://www.cambridge.org/core/product/identifier/S0022112010000297/type/journal_article) doi: 10.1017/S0022112010000297
- Duguet, Y., Willis, A. P., & Kerswell, R. R. (2008, October). Transition in pipe flow: the saddle structure on the boundary of turbulence. *Journal of Fluid Mechanics*, *613*, 255–274. Retrieved 2025-04-23, from [https://www.cambridge.org/core/product/identifier/S0022112008003248/type/journal\\_article](https://www.cambridge.org/core/product/identifier/S0022112008003248/type/journal_article) doi: 10.1017/S0022112008003248
- Ecke, R. E., Hu, Y., Mainieri, R., & Ahlers, G. (1995, September). Excitation of Spirals and Chiral Symmetry Breaking in Rayleigh-Bénard Convection. *Science*, *269*(5231), 1704–1707. Retrieved 2025-03-25, from <https://www.science.org/doi/10.1126/science.269.5231.1704> doi: 10.1126/science.269.5231.1704
- Eckhaus, W. (1965). *Studies in Non-Linear Stability Theory* (Vol. 6; C. Truesdell, L. Collatz, G. Fichera, P. Germain, J. Keller, & A. Seeger, Eds.). Berlin, Heidelberg: Springer

- Berlin Heidelberg. Retrieved 2025-04-01, from <http://link.springer.com/10.1007/978-3-642-88317-0> doi: 10.1007/978-3-642-88317-0
- Egolf, D. A., Melnikov, I. V., & Bodenschatz, E. (1998, April). Importance of Local Pattern Properties in Spiral Defect Chaos. *Physical Review Letters*, 80(15), 3228–3231. Retrieved 2025-03-25, from <https://link.aps.org/doi/10.1103/PhysRevLett.80.3228> doi: 10.1103/PhysRevLett.80.3228
- Egolf, D. A., Melnikov, I. V., Pesch, W., & Ecke, R. E. (2000, April). Mechanisms of extensive spatiotemporal chaos in Rayleigh–Bénard convection. *Nature*, 404(6779), 733–736. Retrieved 2025-03-25, from <https://www.nature.com/articles/35008013> doi: 10.1038/35008013
- Ellingsen, T., & Palm, E. (1975, April). Stability of linear flow. *The Physics of Fluids*, 18(4), 487–488. Retrieved 2025-04-07, from <https://pubs.aip.org/pfl/article/18/4/487/459138/Stability-of-linear-flow> doi: 10.1063/1.861156
- Evans, G., & Greif, R. (1991, August). Unsteady three-dimensional mixed convection in a heated horizontal channel with applications to chemical vapor deposition. *International Journal of Heat and Mass Transfer*, 34(8), 2039–2051. Retrieved 2025-03-25, from <https://linkinghub.elsevier.com/retrieve/pii/001793109190215Z> doi: 10.1016/0017-9310(91)90215-Z
- Faisst, H., & Eckhardt, B. (2003, November). Traveling Waves in Pipe Flow. *Physical Review Letters*, 91(22), 224502. Retrieved 2025-04-23, from <https://link.aps.org/doi/10.1103/PhysRevLett.91.224502> doi: 10.1103/PhysRevLett.91.224502
- Faisst, H., & Eckhardt, B. (2004, April). Sensitive dependence on initial conditions in transition to turbulence in pipe flow. *Journal of Fluid Mechanics*, 504, 343–352. Retrieved 2025-05-26, from [http://www.journals.cambridge.org/abstract\\_S0022112004008134](http://www.journals.cambridge.org/abstract_S0022112004008134) doi: 10.1017/S0022112004008134
- Farrell, B. F. (1988, August). Optimal excitation of perturbations in viscous shear flow. *The Physics of Fluids*, 31(8), 2093–2102. Retrieved 2025-04-07, from <https://pubs.aip.org/pfl/article/31/8/2093/966463/Optimal-excitation-of-perturbations-in-viscous> doi: 10.1063/1.866609
- Feigenbaum, M. J. (1979). The universal metric properties of nonlinear transformations. *Journal of Statistical Physics*, 21, 669–706. (Publisher: Springer)
- Foias, C., Sell, G. R., & Temam, R. (1988, June). Inertial manifolds for nonlinear evolutionary equations. *Journal of Differential Equations*, 73(2), 309–353. Retrieved 2025-04-24, from <https://linkinghub.elsevier.com/retrieve/pii/0022039688901106> doi: 10.1016/0022-0396(88)90110-6
- Fukui, K., Nakajima, M., & Ueda, H. (1983, January). The longitudinal vortex and its effects on the transport processes in combined free and forced laminar convection between horizontal and inclined parallel plates. *International Journal of Heat and Mass Transfer*, 26(1), 109–120. Retrieved 2025-04-15, from <https://linkinghub.elsevier.com/retrieve/pii/S0017931083800131> doi: 10.1016/S0017-9310(83)80013-1

- Gage, K. S., & Reid, W. H. (1968, July). The stability of thermally stratified plane Poiseuille flow. *Journal of Fluid Mechanics*, 33(1), 21–32. Retrieved 2025-03-25, from [https://www.cambridge.org/core/product/identifier/S0022112068002326/type/journal\\_article](https://www.cambridge.org/core/product/identifier/S0022112068002326/type/journal_article) doi: 10.1017/S0022112068002326
- Gibson, J. F., Halcrow, J., & Cvitanović, P. (2008, September). Visualizing the geometry of state space in plane Couette flow. *Journal of Fluid Mechanics*, 611, 107–130. Retrieved 2025-04-07, from [https://www.cambridge.org/core/product/identifier/S002211200800267X/type/journal\\_article](https://www.cambridge.org/core/product/identifier/S002211200800267X/type/journal_article) doi: 10.1017/S002211200800267X
- Gibson, J. F., Halcrow, J., & Cvitanović, P. (2009, November). Equilibrium and travelling-wave solutions of plane Couette flow. *Journal of Fluid Mechanics*, 638, 243–266. Retrieved 2025-04-07, from [https://www.cambridge.org/core/product/identifier/S0022112009990863/type/journal\\_article](https://www.cambridge.org/core/product/identifier/S0022112009990863/type/journal_article) doi: 10.1017/S0022112009990863
- Gollub, J. P., & Swinney, H. L. (1975, October). Onset of Turbulence in a Rotating Fluid. *Physical Review Letters*, 35(14), 927–930. Retrieved 2025-04-24, from <https://link.aps.org/doi/10.1103/PhysRevLett.35.927> doi: 10.1103/PhysRevLett.35.927
- Gomé, S., Tuckerman, L. S., & Barkley, D. (2020, August). Statistical transition to turbulence in plane channel flow. *Physical Review Fluids*, 5(8), 083905. Retrieved 2025-03-25, from <https://link.aps.org/doi/10.1103/PhysRevFluids.5.083905> doi: 10.1103/PhysRevFluids.5.083905
- Graham, M. D., & Floryan, D. (2021, January). Exact Coherent States and the Nonlinear Dynamics of Wall-Bounded Turbulent Flows. *Annual Review of Fluid Mechanics*, 53(1), 227–253. Retrieved 2025-04-07, from <https://www.annualreviews.org/doi/10.1146/annurev-fluid-051820-020223> doi: 10.1146/annurev-fluid-051820-020223
- Halcrow, J., Gibson, J. F., Cvitanović, P., & Viswanath, D. (2009, February). Heteroclinic connections in plane Couette flow. *Journal of Fluid Mechanics*, 621, 365–376. Retrieved 2025-04-07, from [https://www.cambridge.org/core/product/identifier/S0022112008005065/type/journal\\_article](https://www.cambridge.org/core/product/identifier/S0022112008005065/type/journal_article) doi: 10.1017/S0022112008005065
- Hall, P., & Sherwin, S. (2010, October). Streamwise vortices in shear flows: harbingers of transition and the skeleton of coherent structures. *Journal of Fluid Mechanics*, 661, 178–205. Retrieved 2025-10-31, from [https://www.cambridge.org/core/product/identifier/S0022112010002892/type/journal\\_article](https://www.cambridge.org/core/product/identifier/S0022112010002892/type/journal_article) doi: 10.1017/S0022112010002892
- Hall, P., & Smith, F. T. (1988, June). The nonlinear interaction of Tollmien–Schlichting waves and Taylor–Görtler vortices in curved channel flows. *Proceedings of the Royal Society of London. A. Mathematical and Physical Sciences*, 417(1853), 255–282. Retrieved 2025-10-31, from <https://royalsocietypublishing.org/doi/10.1098/rspa.1988.0060> doi: 10.1098/rspa.1988.0060
- Hall, P., & Smith, F. T. (1990). Near-Planar Ts Waves and Longitudinal Vortices in Channel Flow: Nonlinear Interaction and Focussing. In B. A. Stewart, R. Lal, & B. A. Stewart (Eds.), *Soil Restoration* (Vol. 17, pp. 5–39). New York, NY: Springer New York. Retrieved 2025-10-31, from [http://link.springer.com/10.1007/978-1-4612-3432-6\\_2](http://link.springer.com/10.1007/978-1-4612-3432-6_2) (Series Title:

- Advances in Soil Science) doi: 10.1007/978-1-4612-3432-6\_2
- Hall, P., & Smith, F. T. (1991, June). On strongly nonlinear vortex/wave interactions in boundary-layer transition. *Journal of Fluid Mechanics*, 227, 641–666. Retrieved 2025-10-31, from [https://www.cambridge.org/core/product/identifier/S0022112091000289/type/journal\\_article](https://www.cambridge.org/core/product/identifier/S0022112091000289/type/journal_article) doi: 10.1017/S0022112091000289
- Hamilton, J. M., Kim, J., & Waleffe, F. (1995, March). Regeneration mechanisms of near-wall turbulence structures. *Journal of Fluid Mechanics*, 287, 317–348. Retrieved 2025-04-07, from [https://www.cambridge.org/core/product/identifier/S0022112095000978/type/journal\\_article](https://www.cambridge.org/core/product/identifier/S0022112095000978/type/journal_article) doi: 10.1017/S0022112095000978
- Hoard, C., Robertson, C., & Acrivos, A. (1970, May). Experiments on the cellular structure in bénard convection. *International Journal of Heat and Mass Transfer*, 13(5), 849–856. Retrieved 2025-04-01, from <https://linkinghub.elsevier.com/retrieve/pii/0017931070901304> doi: 10.1016/0017-9310(70)90130-4
- Hof, B., Lucas, P. G. J., & Mullin, T. (1999, October). Flow state multiplicity in convection. *Physics of Fluids*, 11(10), 2815–2817. Retrieved 2025-03-25, from <https://pubs.aip.org/pof/article/11/10/2815/254396/Flow-state-multiplicity-in-convection> doi: 10.1063/1.870178
- Hof, B., Westerweel, J., Schneider, T. M., & Eckhardt, B. (2006, September). Finite lifetime of turbulence in shear flows. *Nature*, 443(7107), 59–62. Retrieved 2025-04-25, from <https://www.nature.com/articles/nature05089> doi: 10.1038/nature05089
- Hopf, E. (1948, December). A mathematical example displaying features of turbulence. *Communications on Pure and Applied Mathematics*, 1(4), 303–322. Retrieved 2025-04-24, from <https://onlinelibrary.wiley.com/doi/10.1002/cpa.3160010401> doi: 10.1002/cpa.3160010401
- Hossain, M. Z., Floryan, D., & Floryan, J. M. (2012, December). Drag reduction due to spatial thermal modulations. *Journal of Fluid Mechanics*, 713, 398–419. Retrieved 2025-03-25, from [https://www.cambridge.org/core/product/identifier/S002211201200465X/type/journal\\_article](https://www.cambridge.org/core/product/identifier/S002211201200465X/type/journal_article) doi: 10.1017/jfm.2012.465
- Hossain, M. Z., & Floryan, J. M. (2016, March). Drag reduction in a thermally modulated channel. *Journal of Fluid Mechanics*, 791, 122–153. Retrieved 2025-03-25, from [https://www.cambridge.org/core/product/identifier/S0022112016000422/type/journal\\_article](https://www.cambridge.org/core/product/identifier/S0022112016000422/type/journal_article) doi: 10.1017/jfm.2016.42
- Hossain, M. Z., & Floryan, J. M. (2020, August). On the role of surface grooves in the reduction of pressure losses in heated channels. *Physics of Fluids*, 32(8), 083610. Retrieved 2025-03-25, from <https://pubs.aip.org/pof/article/32/8/083610/1060903/On-the-role-of-surface-grooves-in-the-reduction-of> doi: 10.1063/5.0018416
- Hu, Y., Ecke, R., & Ahlers, G. (1993, December). Convection near threshold for Prandtl numbers near 1. *Physical Review E*, 48(6), 4399–4413. Retrieved 2025-03-25, from <https://link.aps.org/doi/10.1103/PhysRevE.48.4399> doi: 10.1103/PhysRevE.48.4399
- Hu, Y., Ecke, R., & Ahlers, G. (1995, April). Convection for Prandtl numbers near 1: Dynamics of

- textured patterns. *Physical Review E*, 51(4), 3263–3279. Retrieved 2025-03-25, from <https://link.aps.org/doi/10.1103/PhysRevE.51.3263> doi: 10.1103/PhysRevE.51.3263
- Hu, Y., Ecke, R. E., & Ahlers, G. (1997, June). Convection under rotation for Prandtl numbers near 1: Linear stability, wave-number selection, and pattern dynamics. *Physical Review E*, 55(6), 6928–6949. Retrieved 2025-03-25, from <https://link.aps.org/doi/10.1103/PhysRevE.55.6928> doi: 10.1103/PhysRevE.55.6928
- Huerre, P., & Monkewitz, P. A. (1990). Local and global instabilities in spatially developing flows. *Annual review of fluid mechanics*, 22(1), 473–537.
- Hwang, Y., & Cossu, C. (2010, December). Linear non-normal energy amplification of harmonic and stochastic forcing in the turbulent channel flow. *Journal of Fluid Mechanics*, 664, 51–73. Retrieved 2025-04-25, from [https://www.cambridge.org/core/product/identifier/S0022112010003629/type/journal\\_article](https://www.cambridge.org/core/product/identifier/S0022112010003629/type/journal_article) doi: 10.1017/S0022112010003629
- Iida, O., & Nagano, Y. (1998). The Relaminarization Mechanisms of Turbulent Channel Flow at Low Reynolds Numbers. *Flow, Turbulence and Combustion*, 60(2), 193–213. Retrieved 2025-04-25, from <http://link.springer.com/10.1023/A:1009999606355> doi: 10.1023/A:1009999606355
- Jeffreys, H. (1928, March). Some cases of instability in fluid motion. *Proceedings of the Royal Society of London. Series A, Containing Papers of a Mathematical and Physical Character*, 118(779), 195–208. Retrieved 2025-04-13, from <https://royalsocietypublishing.org/doi/10.1098/rspa.1928.0045> doi: 10.1098/rspa.1928.0045
- Jensen, K. F., Einset, E. O., & Fotiadis, D. I. (1991, January). Flow Phenomena in Chemical Vapor Deposition of Thin Films. *Annual Review of Fluid Mechanics*, 23(1), 197–232. Retrieved 2025-03-25, from <https://www.annualreviews.org/doi/10.1146/annurev.fl.23.010191.001213> doi: 10.1146/annurev.fl.23.010191.001213
- John, A., Gunter, F., & Maria, H. (1993, August). Routes to chaos and turbulence. A computational introduction. *Philosophical Transactions of the Royal Society of London. Series A: Physical and Engineering Sciences*, 344(1671), 207–234. Retrieved 2025-04-24, from <https://royalsocietypublishing.org/doi/10.1098/rsta.1993.0088> doi: 10.1098/rsta.1993.0088
- John Soundar Jerome, J., Chomaz, J.-M., & Huerre, P. (2012, April). Transient growth in Rayleigh-Bénard-Poiseuille/Couette convection. *Physics of Fluids*, 24(4), 044103. Retrieved 2025-03-25, from <https://pubs.aip.org/pof/article/24/4/044103/257562/Transient-growth-in-Rayleigh-Benard-Poiseuille> doi: 10.1063/1.4704642
- Karimi, A., Huang, Z.-F., & Paul, M. R. (2011, October). Exploring spiral defect chaos in generalized Swift-Hohenberg models with mean flow. *Physical Review E*, 84(4), 046215. Retrieved 2025-03-25, from <https://link.aps.org/doi/10.1103/PhysRevE.84.046215> doi: 10.1103/PhysRevE.84.046215
- Kashyap, P. V., Duguet, Y., & Dauchot, O. (2022, December). Linear Instability of Turbulent Channel Flow. *Physical Review Letters*, 129(24), 244501. Retrieved 2025-04-25, from <https://link.aps.org/doi/10.1103/PhysRevLett.129.244501> doi: 10.1103/PhysRevLett.129

.244501

- Kawahara, G., & Kida, S. (2001, December). Periodic motion embedded in plane Couette turbulence: regeneration cycle and burst. *Journal of Fluid Mechanics*, 449, 291–300. Retrieved 2025-04-07, from [https://www.cambridge.org/core/product/identifier/S0022112001006243/type/journal\\_article](https://www.cambridge.org/core/product/identifier/S0022112001006243/type/journal_article) doi: 10.1017/S0022112001006243
- Kelly, R. (1994). The Onset and Development of Thermal Convection in Fully Developed Shear Flows. In *Advances in Applied Mechanics* (Vol. 31, pp. 35–112). Elsevier. Retrieved 2025-03-25, from <https://linkinghub.elsevier.com/retrieve/pii/S0065215608702552> doi: 10.1016/S0065-2156(08)70255-2
- Kennedy, K., & Zebib, A. (1983, March). Combined free and forced convection between horizontal parallel planes: some case studies. *International Journal of Heat and Mass Transfer*, 26(3), 471–474. Retrieved 2025-03-25, from <https://linkinghub.elsevier.com/retrieve/pii/0017931083900522> doi: 10.1016/0017-9310(83)90052-2
- Kerswell, R. R., & Tutty, O. R. (2007, August). Recurrence of travelling waves in transitional pipe flow. *Journal of Fluid Mechanics*, 584, 69–102. Retrieved 2025-04-23, from [https://www.cambridge.org/core/product/identifier/S0022112007006301/type/journal\\_article](https://www.cambridge.org/core/product/identifier/S0022112007006301/type/journal_article) doi: 10.1017/S0022112007006301
- Kline, S. J., Reynolds, W. C., Schraub, F. A., & Runstadler, P. W. (1967, December). The structure of turbulent boundary layers. *Journal of Fluid Mechanics*, 30(4), 741–773. Retrieved 2025-03-25, from [https://www.cambridge.org/core/product/identifier/S0022112067001740/type/journal\\_article](https://www.cambridge.org/core/product/identifier/S0022112067001740/type/journal_article) doi: 10.1017/S0022112067001740
- Koschmieder, E., & Pallas, S. (1974, September). Heat transfer through a shallow, horizontal convecting fluid layer. *International Journal of Heat and Mass Transfer*, 17(9), 991–1002. Retrieved 2025-04-11, from <https://linkinghub.elsevier.com/retrieve/pii/0017931074901811> doi: 10.1016/0017-9310(74)90181-1
- Kreilos, T., & Eckhardt, B. (2012, December). Periodic orbits near onset of chaos in plane Couette flow. *Chaos: An Interdisciplinary Journal of Nonlinear Science*, 22(4), 047505. Retrieved 2025-04-07, from <https://pubs.aip.org/cha/article/22/4/047505/341745/Periodic-orbits-near-onset-of-chaos-in-plane> doi: 10.1063/1.4757227
- Lai, Y.-C., & Tél, T. (2011). *Transient Chaos* (Vol. 173). New York, NY: Springer New York. Retrieved 2025-05-26, from <http://link.springer.com/10.1007/978-1-4419-6987-3> doi: 10.1007/978-1-4419-6987-3
- Landau, L. D. (1944). On the problem of turbulence. In (Vol. 44, p. 311).
- Le Gal, P., Pocheau, A., & Croquette, V. (1985, June). Square versus Roll Pattern at Convective Threshold. *Physical Review Letters*, 54(23), 2501–2504. Retrieved 2025-03-25, from <https://link.aps.org/doi/10.1103/PhysRevLett.54.2501> doi: 10.1103/PhysRevLett.54.2501
- Liu, J., & Ahlers, G. (1996). Spiral-Defect Chaos in Rayleigh-Bénard Convection with Small Prandtl Numbers. *PHYSICAL REVIEW LETTERS*, 77(15).
- Lowe, M., & Gollub, J. P. (1985, December). Pattern Selection near the Onset of Convection: The Eckhaus Instability. *Physical Review Letters*, 55(23), 2575–2578. Retrieved 2025-04-

- 15, from <https://link.aps.org/doi/10.1103/PhysRevLett.55.2575> doi: 10.1103/PhysRevLett.55.2575
- Luijkx, J.-M., Platten, J. K., & Legros, J. C. (1981). On the existence of thermoconvective rolls, transverse to a superimposed mean Poiseuille flow. *International Journal of Heat and Mass Transfer*, 24(7), 1287–1291. (Publisher: Elsevier)
- Lustro, J. R. T., Kawahara, G., Van Veen, L., Shimizu, M., & Kokubu, H. (2019, March). The onset of transient turbulence in minimal plane Couette flow. *Journal of Fluid Mechanics*, 862, R2. Retrieved 2025-10-30, from [https://www.cambridge.org/core/product/identifier/S0022112018009710/type/journal\\_article](https://www.cambridge.org/core/product/identifier/S0022112018009710/type/journal_article) doi: 10.1017/jfm.2018.971
- Ma, D.-J., Sun, D.-J., & Yin, X.-Y. (2006, September). Multiplicity of steady states in cylindrical Rayleigh-Bénard convection. *Physical Review E*, 74(3), 037302. Retrieved 2025-03-25, from <https://link.aps.org/doi/10.1103/PhysRevE.74.037302> doi: 10.1103/PhysRevE.74.037302
- Manneville, P. (2006). Rayleigh-Bénard Convection: Thirty Years of Experimental, Theoretical, and Modeling Work. In G. Höhler et al. (Eds.), *Dynamics of Spatio-Temporal Cellular Structures* (Vol. 207, pp. 41–65). New York, NY: Springer New York. Retrieved 2025-03-25, from [http://link.springer.com/10.1007/978-0-387-25111-0\\_3](http://link.springer.com/10.1007/978-0-387-25111-0_3) (Series Title: Springer Tracts in Modern Physics) doi: 10.1007/978-0-387-25111-0\_3
- Manneville, P., & Pomeau, Y. (1979). Intermittency and the Lorenz model. *Physics Letters A*, 75(1-2), 1–2. (Publisher: North-Holland)
- Mellibovsky, F., & Eckhardt, B. (2012). From travelling waves to mild chaos: a supercritical bifurcation cascade in pipe flow. *Journal of Fluid Mechanics*, 709, 149–190. Retrieved from <https://www.cambridge.org/core/product/BE84A18A7FCD05488775E46B3C230844> (Edition: 2012/08/29 Publisher: Cambridge University Press) doi: 10.1017/jfm.2012.326
- Meseguer, A., & Trefethen, L. (2003, March). Linearized pipe flow to Reynolds number 107. *Journal of Computational Physics*, 186(1), 178–197. Retrieved 2025-04-03, from <https://linkinghub.elsevier.com/retrieve/pii/S0021999103000299> doi: 10.1016/S0021-9991(03)00029-9
- Morris, S. W., Bodenschatz, E., Cannell, D. S., & Ahlers, G. (1993, September). Spiral defect chaos in large aspect ratio Rayleigh-Bénard convection. *Physical Review Letters*, 71(13), 2026–2029. Retrieved 2025-03-25, from <https://link.aps.org/doi/10.1103/PhysRevLett.71.2026> doi: 10.1103/PhysRevLett.71.2026
- Morris, S. W., Bodenschatz, E., Cannell, D. S., & Ahlers, G. (1996, October). The spatio-temporal structure of spiral-defect chaos. *Physica D: Nonlinear Phenomena*, 97(1-3), 164–179. Retrieved 2025-03-25, from <https://linkinghub.elsevier.com/retrieve/pii/0167278996000966> doi: 10.1016/0167-2789(96)00096-6
- Müller, H. W., Lücke, M., & Kamps, M. (1992, March). Transversal convection patterns in horizontal shear flow. *Physical Review A*, 45(6), 3714–3726. Retrieved 2025-03-25, from <https://link.aps.org/doi/10.1103/PhysRevA.45.3714> doi: 10.1103/PhysRevA.45.3714
- Nagata, M. (1990, August). Three-dimensional finite-amplitude solutions in plane Couette flow:

- bifurcation from infinity. *Journal of Fluid Mechanics*, 217, 519–527. Retrieved 2025-04-07, from [https://www.cambridge.org/core/product/identifier/S0022112090000829/type/journal\\_article](https://www.cambridge.org/core/product/identifier/S0022112090000829/type/journal_article) doi: 10.1017/S0022112090000829
- Nagata, M. (1997, February). Three-dimensional traveling-wave solutions in plane Couette flow. *Physical Review E*, 55(2), 2023–2025. Retrieved 2025-04-07, from <https://link.aps.org/doi/10.1103/PhysRevE.55.2023> doi: 10.1103/PhysRevE.55.2023
- Nicolas, X. (2002, October). Revue bibliographique sur les écoulements de Poiseuille–Rayleigh–Bénard : écoulements de convection mixte en conduites rectangulaires horizontales chauffées par le bas. *International Journal of Thermal Sciences*, 41(10), 961–1016. Retrieved 2025-03-25, from <https://linkinghub.elsevier.com/retrieve/pii/S1290072902013741> doi: 10.1016/S1290-0729(02)01374-1
- Nicolas, X., Luijkx, J.-M., & Platten, J.-K. (2000, February). Linear stability of mixed convection flows in horizontal rectangular channels of finite transversal extension heated from below. *International Journal of Heat and Mass Transfer*, 43(4), 589–610. Retrieved 2025-04-15, from <https://linkinghub.elsevier.com/retrieve/pii/S001793109900099X> doi: 10.1016/S0017-9310(99)00099-X
- Nicolas, X., Mojtabi, A., & Platten, J. K. (1997, February). Two-dimensional numerical analysis of the Poiseuille–Bénard flow in a rectangular channel heated from below. *Physics of Fluids*, 9(2), 337–348. Retrieved 2025-04-01, from <https://pubs.aip.org/pof/article/9/2/337/259822/Two-dimensional-numerical-analysis-of-the> doi: 10.1063/1.869235
- Nicolas, X., Xin, S., & Zoueidi, N. (2010, January). Characterisation of a Wavy Convective Instability in Poiseuille-Rayleigh-Bénard Flows: Linear Stability Analysis and Non Linear Numerical Simulations Under Random Excitations. In *2010 14th International Heat Transfer Conference, Volume 7* (pp. 203–208). Washington, DC, USA: ASMEDC. Retrieved 2025-03-25, from <https://asmedigitalcollection.asme.org/IHTC/proceedings/IHTC14/49422/203/360332> doi: 10.1115/IHTC14-22256
- Nicolas, X., Zoueidi, N., & Xin, S. (2012, August). Influence of a white noise at channel inlet on the parallel and wavy convective instabilities of Poiseuille-Rayleigh-Bénard flows. *Physics of Fluids*, 24(8), 084101. Retrieved 2025-04-15, from <https://pubs.aip.org/pof/article/24/8/084101/258132/Influence-of-a-white-noise-at-channel-inlet-on-the> doi: 10.1063/1.4737652
- Orr, W. M. (1907). The Stability or Instability of the Steady Motions of a Perfect Liquid and of a Viscous Liquid. Part II: A Viscous Liquid. *Proceedings of the Royal Irish Academy. Section A: Mathematical and Physical Sciences*, 27, 69–138. Retrieved 2025-04-03, from <http://www.jstor.org/stable/20490591> (Publisher: Royal Irish Academy)
- Orszag, S. A. (1971, December). Accurate solution of the Orr–Sommerfeld stability equation. *Journal of Fluid Mechanics*, 50(4), 689–703. Retrieved 2025-03-25, from [https://www.cambridge.org/core/product/identifier/S0022112071002842/type/journal\\_article](https://www.cambridge.org/core/product/identifier/S0022112071002842/type/journal_article) doi: 10.1017/S0022112071002842
- Orszag, S. A., & Patera, A. T. (1983, March). Secondary instability of wall-bounded shear flows.

- Journal of Fluid Mechanics*, 128(-1), 347. Retrieved 2025-03-25, from [http://www.journals.cambridge.org/abstract\\_S0022112083000518](http://www.journals.cambridge.org/abstract_S0022112083000518) doi: 10.1017/S0022112083000518
- Ostrach, S., & Kamotani, Y. (1975, May). Heat Transfer Augmentation in Laminar Fully Developed Channel Flow by Means of Heating From Below. *Journal of Heat Transfer*, 97(2), 220–225. Retrieved 2025-04-15, from <https://asmedigitalcollection.asme.org/heattransfer/article/97/2/220/416581/Heat-Transfer-Augmentation-in-Laminar-Fully> doi: 10.1115/1.3450344
- Ouazzani, M., Caltagirone, J.-P., Meyer, G., & Mojtabi, A. (1989). Etude numerique et expérimentale de la convection mixte entre deux plans horizontaux à températures différentes. *International journal of heat and mass transfer*, 32(2), 261–269. (Publisher: Elsevier)
- Ouazzani, M., Platten, J. K., & Mojtabi, A. (1990). Etude expérimentale de la convection mixte entre deux plans horizontaux à températures différentes—II. *International journal of heat and mass transfer*, 33(7), 1417–1427. (Publisher: Elsevier)
- Pabiou, H., Mergui, S., & Bénard, C. (2005, October). Wavy secondary instability of longitudinal rolls in RayleighPoiseuille flows. *Journal of Fluid Mechanics*, 542(-1), 175. Retrieved 2025-03-25, from [http://www.journals.cambridge.org/abstract\\_S0022112005006154](http://www.journals.cambridge.org/abstract_S0022112005006154) doi: 10.1017/S0022112005006154
- Pabiou, H., Nicolas, X., Xin, S., & Mergui, S. (2003). Observations d'une instabilité convective apparaissant sous la forme de rouleaux sinueux dans un écoulement de Poiseuille–Rayleigh–Bénard. *Mécanique & industries*, 4(5), 537–543. (Publisher: Elsevier)
- Paranjape, C. S. (2019). Onset of turbulence in plane Poiseuille flow. (Publisher: IST Austria Klosterneuburg, Austria)
- Paranjape, C. S., Duguet, Y., & Hof, B. (2020, August). Oblique stripe solutions of channel flow. *Journal of Fluid Mechanics*, 897, A7. Retrieved 2025-04-08, from [https://www.cambridge.org/core/product/identifier/S0022112020003225/type/journal\\_article](https://www.cambridge.org/core/product/identifier/S0022112020003225/type/journal_article) doi: 10.1017/jfm.2020.322
- Paranjape, C. S., Yalnız, G., Duguet, Y., Budanur, N. B., & Hof, B. (2023, July). Direct Path from Turbulence to Time-Periodic Solutions. *Physical Review Letters*, 131(3), 034002. Retrieved 2025-04-08, from <https://link.aps.org/doi/10.1103/PhysRevLett.131.034002> doi: 10.1103/PhysRevLett.131.034002
- Patel, V. C., & Head, M. R. (1969, August). Some observations on skin friction and velocity profiles in fully developed pipe and channel flows. *Journal of Fluid Mechanics*, 38(1), 181–201. Retrieved 2025-03-25, from [https://www.cambridge.org/core/product/identifier/S0022112069000115/type/journal\\_article](https://www.cambridge.org/core/product/identifier/S0022112069000115/type/journal_article) doi: 10.1017/S0022112069000115
- Paul, M., Chiam, K.-H., Cross, M., Fischer, P., & Greenside, H. (2003, October). Pattern formation and dynamics in Rayleigh–Bénard convection: numerical simulations of experimentally realistic geometries. *Physica D: Nonlinear Phenomena*, 184(1-4), 114–126. Retrieved 2025-03-25, from <https://linkinghub.elsevier.com/retrieve/pii/S0167278903002161> doi: 10.1016/S0167-2789(03)00216-1
- Paul, M. R., Einarsson, M. I., Fischer, P. F., & Cross, M. C. (2007, April). Extensive chaos in Rayleigh-

- Bénard convection. *Physical Review E*, 75(4), 045203. Retrieved 2025-03-25, from <https://link.aps.org/doi/10.1103/PhysRevE.75.045203> doi: 10.1103/PhysRevE.75.045203
- Pellew, A., & Southwell, R. V. (1940, November). On maintained convective motion in a fluid heated from below. *Proceedings of the Royal Society of London. Series A. Mathematical and Physical Sciences*, 176(966), 312–343. Retrieved 2025-03-25, from <https://royalsocietypublishing.org/doi/10.1098/rspa.1940.0092> doi: 10.1098/rspa.1940.0092
- Pirozzoli, S., Bernardini, M., Verzicco, R., & Orlandi, P. (2017, June). Mixed convection in turbulent channels with unstable stratification. *Journal of Fluid Mechanics*, 821, 482–516. Retrieved 2025-03-25, from [https://www.cambridge.org/core/product/identifier/S0022112017002166/type/journal\\_article](https://www.cambridge.org/core/product/identifier/S0022112017002166/type/journal_article) doi: 10.1017/jfm.2017.216
- Plapp, B. B. (1997). *Spiral pattern formation in Rayleigh-Bénard convection* (Doctoral dissertation). Retrieved 2025-04-01, from <https://ui.adsabs.harvard.edu/abs/1997PhDT.....105P> (Pages: 3118 Publication Title: Ph.D. Thesis ADS Bibcode: 1997PhDT.....105P)
- Plapp, B. B., & Bodenschatz, E. (1996, January). Core dynamics of multi-armed spirals in Rayleigh-Bénard convection. *Physica Scripta*, T67, 111–116. Retrieved 2025-03-25, from <https://iopscience.iop.org/article/10.1088/0031-8949/1996/T67/022> doi: 10.1088/0031-8949/1996/T67/022
- Plapp, B. B., Egolf, D. A., Bodenschatz, E., & Pesch, W. (1998, December). Dynamics and Selection of Giant Spirals in Rayleigh-Bénard Convection. *Physical Review Letters*, 81(24), 5334–5337. Retrieved 2025-03-25, from <https://link.aps.org/doi/10.1103/PhysRevLett.81.5334> doi: 10.1103/PhysRevLett.81.5334
- Prigent, A., & Dauchot, O. (2002, June). "Barber pole turbulence" in large aspect ratio Taylor-Couette flow. *Physical Review Letters*, 89(1), 014501. Retrieved 2025-04-08, from <http://arxiv.org/abs/cond-mat/0009241> (arXiv:cond-mat/0009241) doi: 10.1103/PhysRevLett.89.014501
- Prigent, A., Grégoire, G., Chaté, H., & Dauchot, O. (2003, January). Long-wavelength modulation of turbulent shear flows. *Physica D: Nonlinear Phenomena*, 174(1-4), 100–113. Retrieved 2025-04-08, from <https://linkinghub.elsevier.com/retrieve/pii/S0167278902006851> doi: 10.1016/S0167-2789(02)00685-1
- Pringle, C. C., Duguet, Y., & Kerswell, R. R. (2009, February). Highly symmetric travelling waves in pipe flow. *Philosophical Transactions of the Royal Society A: Mathematical, Physical and Engineering Sciences*, 367(1888), 457–472. Retrieved 2025-04-23, from <https://royalsocietypublishing.org/doi/10.1098/rsta.2008.0236> doi: 10.1098/rsta.2008.0236
- Pujals, G., García-Villalba, M., Cossu, C., & Depardon, S. (2009, January). A note on optimal transient growth in turbulent channel flows. *Physics of Fluids*, 21(1), 015109. Retrieved 2025-04-25, from <https://pubs.aip.org/pof/article/21/1/015109/256743/A-note-on-optimal-transient-growth-in-turbulent> doi: 10.1063/1.3068760
- Ray, S., & Srinivasan, J. (1992, April). Analysis of conjugate laminar mixed convection cooling in

- a shrouded array of electronic components. *International Journal of Heat and Mass Transfer*, 35(4), 815–822. Retrieved 2025-03-25, from <https://linkinghub.elsevier.com/retrieve/pii/001793109290249R> doi: 10.1016/0017-9310(92)90249-R
- Rayleigh, L. (1916, December). LIX. *On convection currents in a horizontal layer of fluid, when the higher temperature is on the under side*. *The London, Edinburgh, and Dublin Philosophical Magazine and Journal of Science*, 32(192), 529–546. Retrieved 2025-03-25, from <https://www.tandfonline.com/doi/full/10.1080/14786441608635602> doi: 10.1080/14786441608635602
- Reddy, S. C., & Henningson, D. S. (1993, July). Energy growth in viscous channel flows. *Journal of Fluid Mechanics*, 252, 209–238. Retrieved 2025-03-25, from [https://www.cambridge.org/core/product/identifier/S0022112093003738/type/journal\\_article](https://www.cambridge.org/core/product/identifier/S0022112093003738/type/journal_article) doi: 10.1017/S0022112093003738
- Reddy, S. C., Schmid, P. J., & Henningson, D. S. (1993, February). Pseudospectra of the Orr–Sommerfeld Operator. *SIAM Journal on Applied Mathematics*, 53(1), 15–47. Retrieved 2025-04-07, from <http://pubs.siam.org/doi/10.1137/0153002> doi: 10.1137/0153002
- Reetz, F., Kreilos, T., & Schneider, T. M. (2019, May). Exact invariant solution reveals the origin of self-organized oblique turbulent-laminar stripes. *Nature Communications*, 10(1), 2277. Retrieved from <https://doi.org/10.1038/s41467-019-10208-x> doi: 10.1038/s41467-019-10208-x
- Reetz, F., & Schneider, T. M. (2020, September). Invariant states in inclined layer convection. Part 1. Temporal transitions along dynamical connections between invariant states. *Journal of Fluid Mechanics*, 898, A22. Retrieved 2025-03-25, from [https://www.cambridge.org/core/product/identifier/S0022112020003171/type/journal\\_article](https://www.cambridge.org/core/product/identifier/S0022112020003171/type/journal_article) doi: 10.1017/jfm.2020.317
- Reetz, F., Subramanian, P., & Schneider, T. M. (2020, September). Invariant states in inclined layer convection. Part 2. Bifurcations and connections between branches of invariant states. *Journal of Fluid Mechanics*, 898, A23. Retrieved 2025-03-25, from [https://www.cambridge.org/core/product/identifier/S0022112020003183/type/journal\\_article](https://www.cambridge.org/core/product/identifier/S0022112020003183/type/journal_article) doi: 10.1017/jfm.2020.318
- Reynolds, O. (1883, December). An experimental investigation of the circumstances which determine whether the motion of water shall be direct or sinuous, and of the law of resistance in parallel channels. *Philosophical Transactions of the Royal Society of London*, 174, 935–982. Retrieved 2025-04-03, from <https://royalsocietypublishing.org/doi/10.1098/rstl.1883.0029> doi: 10.1098/rstl.1883.0029
- Reynolds, O. (1895, December). On the dynamical theory of incompressible viscous fluids and the determination of the criterion. *Philosophical Transactions of the Royal Society of London*. (A.), 186, 123–164. Retrieved 2025-03-25, from <https://royalsocietypublishing.org/doi/10.1098/rsta.1895.0004> doi: 10.1098/rsta.1895.0004
- Rossby, H. T. (1969, April). A study of Bénard convection with and without rotation. *Journal*

- of Fluid Mechanics*, 36(2), 309–335. Retrieved 2025-03-25, from [https://www.cambridge.org/core/product/identifier/S0022112069001674/type/journal\\_article](https://www.cambridge.org/core/product/identifier/S0022112069001674/type/journal_article) doi: 10.1017/S0022112069001674
- Ruelle, D., & Takens, F. (1971, September). On the nature of turbulence. *Communications in Mathematical Physics*, 20(3), 167–192. Retrieved 2025-04-24, from <http://link.springer.com/10.1007/BF01646553> doi: 10.1007/BF01646553
- Rüdiger, S., & Feudel, F. (2000, October). Pattern formation in Rayleigh-Bénard convection in a cylindrical container. *Physical Review E*, 62(4), 4927–4931. Retrieved 2025-03-25, from <https://link.aps.org/doi/10.1103/PhysRevE.62.4927> doi: 10.1103/PhysRevE.62.4927
- Scagliarini, A., Einarsson, H., Gylfason, Á., & Toschi, F. (2015, October). Law of the wall in an unstably stratified turbulent channel flow. *Journal of Fluid Mechanics*, 781, R5. Retrieved 2025-03-25, from [https://www.cambridge.org/core/product/identifier/S002211201500498X/type/journal\\_article](https://www.cambridge.org/core/product/identifier/S002211201500498X/type/journal_article) doi: 10.1017/jfm.2015.498
- Scagliarini, A., Gylfason, A., & Toschi, F. (2014, April). Heat flux scaling in turbulent Rayleigh-Bénard convection with an imposed longitudinal wind. *Physical Review E*, 89(4), 043012. Retrieved 2025-03-25, from <http://arxiv.org/abs/1311.4598> (arXiv:1311.4598 [physics]) doi: 10.1103/PhysRevE.89.043012
- Schlichting, H. (1933). Zur Entstehung der Turbulenz bei der Plattenströmung. *Nachrichten von der Gesellschaft der Wissenschaften zu Göttingen, Mathematisch-Physikalische Klasse*, 1933, 181–208. Retrieved from <http://eudml.org/doc/59420>
- Schlichting, H., & Gersten, K. (2017). Onset of Turbulence (Stability Theory). In *Boundary-Layer Theory* (pp. 415–496). Berlin, Heidelberg: Springer Berlin Heidelberg. Retrieved 2025-04-05, from [http://link.springer.com/10.1007/978-3-662-52919-5\\_15](http://link.springer.com/10.1007/978-3-662-52919-5_15) doi: 10.1007/978-3-662-52919-5\_15
- Schlüter, A., Lortz, D., & Busse, F. (1965, September). On the stability of steady finite amplitude convection. *Journal of Fluid Mechanics*, 23(01), 129. Retrieved 2025-03-25, from [http://www.journals.cambridge.org/abstract\\_S0022112065001271](http://www.journals.cambridge.org/abstract_S0022112065001271) doi: 10.1017/S0022112065001271
- Schmid, P. J. (2007, January). Nonmodal Stability Theory. *Annual Review of Fluid Mechanics*, 39(1), 129–162. Retrieved 2025-04-03, from <https://www.annualreviews.org/doi/10.1146/annurev.fluid.38.050304.092139> doi: 10.1146/annurev.fluid.38.050304.092139
- Schmid, P. J., & Henningson, D. S. (2001). *Stability and Transition in Shear Flows* (Vol. 142; J. E. Marsden & L. Sirovich, Eds.). New York, NY: Springer New York. Retrieved 2025-04-03, from <http://link.springer.com/10.1007/978-1-4613-0185-1> doi: 10.1007/978-1-4613-0185-1
- Schmitz, R., Pesch, W., & Zimmermann, W. (2002, March). Spiral-defect chaos: Swift-Hohenberg model versus Boussinesq equations. *Physical Review E*, 65(3), 037302. Retrieved 2025-03-25, from <https://link.aps.org/doi/10.1103/PhysRevE.65.037302> doi: 10.1103/PhysRevE.65.037302

- Schneider, T. M., & Eckhardt, B. (2009, February). Edge states intermediate between laminar and turbulent dynamics in pipe flow. *Philosophical Transactions of the Royal Society A: Mathematical, Physical and Engineering Sciences*, 367(1888), 577–587. Retrieved 2025-04-23, from <https://royalsocietypublishing.org/doi/10.1098/rsta.2008.0216> doi: 10.1098/rsta.2008.0216
- Schneider, T. M., Eckhardt, B., & Yorke, J. A. (2007, July). Turbulence transition and the edge of chaos in pipe flow. *Physical Review Letters*, 99(3), 034502. Retrieved 2025-03-25, from <http://arxiv.org/abs/nlin/0703067> (arXiv:nlin/0703067) doi: 10.1103/PhysRevLett.99.034502
- Shimizu, M., & Manneville, P. (2019, November). Bifurcations to turbulence in transitional channel flow. *Physical Review Fluids*, 4(11), 113903. Retrieved from <https://link.aps.org/doi/10.1103/PhysRevFluids.4.113903> (Publisher: American Physical Society) doi: 10.1103/PhysRevFluids.4.113903
- Siggens, J. H. (2003, January). Dynamics of target patterns in low-Prandtl-number convection. *Journal of Fluid Mechanics*, 475, 357–375. Retrieved 2025-03-25, from [https://www.cambridge.org/core/product/identifier/S0022112002002896/type/journal\\_article](https://www.cambridge.org/core/product/identifier/S0022112002002896/type/journal_article) doi: 10.1017/S0022112002002896
- Smith, C. R., & Metzler, S. P. (1983, April). The characteristics of low-speed streaks in the near-wall region of a turbulent boundary layer. *Journal of Fluid Mechanics*, 129(-1), 27. Retrieved 2025-03-25, from [http://www.journals.cambridge.org/abstract\\_S0022112083000634](http://www.journals.cambridge.org/abstract_S0022112083000634) doi: 10.1017/S0022112083000634
- Sommerfeld, A. (1909). *Ein Beitrag zur hydrodynamischen Erklärung der turbulenten Flüssigkeitsbewegungen*.
- Song, B., Barkley, D., Hof, B., & Avila, M. (2017, February). Speed and structure of turbulent fronts in pipe flow. *Journal of Fluid Mechanics*, 813, 1045–1059. Retrieved 2025-04-08, from [https://www.cambridge.org/core/product/identifier/S0022112017000143/type/journal\\_article](https://www.cambridge.org/core/product/identifier/S0022112017000143/type/journal_article) doi: 10.1017/jfm.2017.14
- Squire, H. B. (1933, November). On the stability for three-dimensional disturbances of viscous fluid flow between parallel walls. *Proceedings of the Royal Society of London. Series A, Containing Papers of a Mathematical and Physical Character*, 142(847), 621–628. Retrieved 2025-03-25, from <https://royalsocietypublishing.org/doi/10.1098/rspa.1933.0193> doi: 10.1098/rspa.1933.0193
- Swift, J., & Hohenberg, P. C. (1977, January). Hydrodynamic fluctuations at the convective instability. *Physical Review A*, 15(1), 319–328. Retrieved 2025-03-25, from <https://link.aps.org/doi/10.1103/PhysRevA.15.319> doi: 10.1103/PhysRevA.15.319
- Swinney, H. L., & Gollub, J. P. (1978). The transition to turbulence. *Physics today*, 31(8), 41–49. (Publisher: American Institute of Physics)
- Tao, J. J., Eckhardt, B., & Xiong, X. M. (2018, January). Extended localized structures and the onset of turbulence in channel flow. *Physical Review Fluids*, 3(1), 011902. Retrieved from <https://link.aps.org/doi/10.1103/PhysRevFluids.3.011902> (Publisher: American Physical

- Society) doi: 10.1103/PhysRevFluids.3.011902
- Toh, S., & Itano, T. (2003, April). A periodic-like solution in channel flow. *Journal of Fluid Mechanics*, 481, 67–76. Retrieved 2025-04-07, from [http://www.journals.cambridge.org/abstract\\_S0022112003003768](http://www.journals.cambridge.org/abstract_S0022112003003768) doi: 10.1017/S0022112003003768
- Tollmien, W. (1928). Über die Entstehung der Turbulenz. 1. Mitteilung. *Nachrichten von der Gesellschaft der Wissenschaften zu Göttingen, Mathematisch-Physikalische Klasse*, 1929, 21–44. Retrieved from <http://eudml.org/doc/59276>
- Trefethen, L. N. (1997, January). Pseudospectra of Linear Operators. *SIAM Review*, 39(3), 383–406. Retrieved 2025-04-07, from <http://pubs.siam.org/doi/10.1137/S0036144595295284> doi: 10.1137/S0036144595295284
- Tsukahara, T., Iwamoto, K., Kawamura, H., & Takeda, T. (2014, September). *DNS of heat transfer in a transitional channel flow accompanied by a turbulent puff-like structure*. arXiv. Retrieved 2025-03-25, from <http://arxiv.org/abs/1406.0586> (arXiv:1406.0586 [physics]) doi: 10.48550/arXiv.1406.0586
- Tsukahara, T., Kawaguchi, Y., & Kawamura, H. (2014). *An experimental study on turbulent-stripe structure in transitional channel flow*. arXiv. Retrieved 2025-04-09, from <https://arxiv.org/abs/1406.1378> (Version Number: 2) doi: 10.48550/ARXIV.1406.1378
- Tsukahara, T., Seki, Y., Kawamura, H., & Tochio, D. (2014, September). *DNS of turbulent channel flow at very low Reynolds numbers*. arXiv. Retrieved 2025-03-25, from <http://arxiv.org/abs/1406.0248> (arXiv:1406.0248 [physics]) doi: 10.48550/arXiv.1406.0248
- Tuckerman, L. S., & Barkley, D. (1988, July). Global Bifurcation to Traveling Waves in Axisymmetric Convection. *Physical Review Letters*, 61(4), 408–411. Retrieved 2025-03-25, from <https://link.aps.org/doi/10.1103/PhysRevLett.61.408> doi: 10.1103/PhysRevLett.61.408
- Tuckerman, L. S., & Barkley, D. (2011). Patterns and dynamics in transitional plane Couette flow. *Physics of Fluids*, 23(4). (Publisher: AIP Publishing)
- Tuckerman, L. S., Kreilos, T., Schröbsdorff, H., Schneider, T. M., & Gibson, J. F. (2014, November). Turbulent-laminar patterns in plane Poiseuille flow. *Physics of Fluids*, 26(11), 114103. Retrieved 2025-03-25, from <https://pubs.aip.org/pof/article/26/11/114103/315350/Turbulent-laminar-patterns-in-plane-Poiseuille> doi: 10.1063/1.4900874
- Vallis, G. K., Parker, D. J., & Tobias, S. M. (2019, March). A simple system for moist convection: the Rainy–Bénard model. *Journal of Fluid Mechanics*, 862, 162–199. Retrieved 2025-04-10, from [https://www.cambridge.org/core/product/identifier/S0022112018009540/type/journal\\_article](https://www.cambridge.org/core/product/identifier/S0022112018009540/type/journal_article) doi: 10.1017/jfm.2018.954
- Van Dyke, M., & Van Dyke, M. (1982). *An album of fluid motion* (Vol. 176). Parabolic Press Stanford.
- Van Veen, L., & Kawahara, G. (2011, September). Homoclinic Tangle on the Edge of Shear Turbulence. *Physical Review Letters*, 107(11), 114501. Retrieved 2025-10-30, from <https://link.aps.org/doi/10.1103/PhysRevLett.107.114501> doi: 10.1103/PhysRevLett.107.114501
- Viswanath, D. (2007, June). Recurrent motions within plane Couette turbulence. *Journal of Fluid Mechanics*, 580, 339–358. Retrieved 2025-04-08, from <https://www.cambridge.org>

- .org/core/product/identifier/S0022112007005459/type/journal\_article doi: 10.1017/S0022112007005459
- Vitral, E., Mukherjee, S., Leo, P. H., Viñals, J., Paul, M. R., & Huang, Z.-F. (2020, September). Spiral defect chaos in Rayleigh-Bénard convection: Asymptotic and numerical studies of azimuthal flows induced by rotating spirals. *Physical Review Fluids*, 5(9), 093501. Retrieved 2025-03-25, from <https://link.aps.org/doi/10.1103/PhysRevFluids.5.093501> doi: 10.1103/PhysRevFluids.5.093501
- Waleffe, F. (1997, April). On a self-sustaining process in shear flows. *Physics of Fluids*, 9(4), 883–900. Retrieved 2025-10-31, from <https://pubs.aip.org/pof/article/9/4/883/260272/On-a-self-sustaining-process-in-shear-flows> doi: 10.1063/1.869185
- Waleffe, F. (2001, May). Exact coherent structures in channel flow. *Journal of Fluid Mechanics*, 435, 93–102. Retrieved 2025-04-07, from [https://www.cambridge.org/core/product/identifier/S0022112001004189/type/journal\\_article](https://www.cambridge.org/core/product/identifier/S0022112001004189/type/journal_article) doi: 10.1017/S0022112001004189
- Waleffe, F. (2003, June). Homotopy of exact coherent structures in plane shear flows. *Physics of Fluids*, 15(6), 1517–1534. Retrieved 2025-04-07, from <https://pubs.aip.org/pof/article/15/6/1517/448391/Homotopy-of-exact-coherent-structures-in-plane> doi: 10.1063/1.1566753
- Waleffe, F., Kim, J., & Hamilton, J. M. (1993). On the Origin of Streaks in Turbulent Shear Flows. In F. Durst, R. Friedrich, B. E. Launder, F. W. Schmidt, U. Schumann, & J. H. Whitelaw (Eds.), *Turbulent Shear Flows 8* (pp. 37–49). Berlin, Heidelberg: Springer Berlin Heidelberg. Retrieved 2025-10-31, from [http://link.springer.com/10.1007/978-3-642-77674-8\\_4](http://link.springer.com/10.1007/978-3-642-77674-8_4) doi: 10.1007/978-3-642-77674-8\_4
- Wang, J., Gibson, J., & Waleffe, F. (2007, May). Lower Branch Coherent States in Shear Flows: Transition and Control. *Physical Review Letters*, 98(20), 204501. Retrieved 2025-04-23, from <https://link.aps.org/doi/10.1103/PhysRevLett.98.204501> doi: 10.1103/PhysRevLett.98.204501
- Wedin, H., & Kerswell, R. R. (2004, June). Exact coherent structures in pipe flow: travelling wave solutions. *Journal of Fluid Mechanics*, 508, 333–371. Retrieved 2025-04-23, from [http://www.journals.cambridge.org/abstract\\_S0022112004009346](http://www.journals.cambridge.org/abstract_S0022112004009346) doi: 10.1017/S0022112004009346
- Wesfreid, J. E. (2017, June). Henri Bénard: Thermal convection and vortex shedding. *Comptes Rendus. Mécanique*, 345(7), 446–466. Retrieved 2025-04-13, from <https://comptes-rendus.academie-sciences.fr/mecanique/articles/10.1016/j.crme.2017.06.006/> doi: 10.1016/j.crme.2017.06.006
- Willis, G. E., & Deardorff, J. W. (1970, December). The oscillatory motions of Rayleigh convection. *Journal of Fluid Mechanics*, 44(04), 661. Retrieved 2025-03-25, from [http://www.journals.cambridge.org/abstract\\_S0022112070002070](http://www.journals.cambridge.org/abstract_S0022112070002070) doi: 10.1017/S0022112070002070
- Xi, H., & Gunton, J. D. (1995, November). Spatiotemporal chaos in a model of Rayleigh-Bénard convection. *Physical Review E*, 52(5), 4963–4975. Retrieved 2025-03-25, from <https://link.aps.org/doi/10.1103/PhysRevE.52.4963> doi: 10.1103/PhysRevE.52.4963

- [link.aps.org/doi/10.1103/PhysRevE.52.4963](https://link.aps.org/doi/10.1103/PhysRevE.52.4963) doi: 10.1103/PhysRevE.52.4963
- Xi, H.-w., Gunton, J. D., & Viñals, J. (1993, September). Spiral defect chaos in a model of Rayleigh-Bénard convection. *Physical Review Letters*, 71(13), 2030–2033. Retrieved 2025-03-25, from <https://link.aps.org/doi/10.1103/PhysRevLett.71.2030> doi: 10.1103/PhysRevLett.71.2030
- Xiao, X., & Song, B. (2020, January). The growth mechanism of turbulent bands in channel flow at low Reynolds numbers. *Journal of Fluid Mechanics*, 883, R1. Retrieved 2025-04-09, from [https://www.cambridge.org/core/product/identifier/S0022112019008991/type/journal\\_article](https://www.cambridge.org/core/product/identifier/S0022112019008991/type/journal_article) doi: 10.1017/jfm.2019.899
- Xin, S., Nicolas, X., & Quéré, P. L. (2006, July). Stability analyses of Longitudinal Rolls of Poiseuille-Rayleigh-Bénard Flows in Air-Filled Channels of Finite Transversal Extension. *Numerical Heat Transfer, Part A: Applications*, 50(5), 467–490. Retrieved 2025-03-25, from <http://www.tandfonline.com/doi/abs/10.1080/10407780600620079> doi: 10.1080/10407780600620079
- Xiong, X., Tao, J., Chen, S., & Brandt, L. (2015, April). Turbulent bands in plane-Poiseuille flow at moderate Reynolds numbers. *Physics of Fluids*, 27(4), 041702. Retrieved 2025-04-09, from <https://pubs.aip.org/pof/article/27/4/041702/1019208/Turbulent-bands-in-plane-Poiseuille-flow-at> doi: 10.1063/1.4917173
- Zammert, S., & Eckhardt, B. (2015, April). Crisis bifurcations in plane Poiseuille flow. *Physical Review E*, 91(4), 041003. Retrieved 2025-03-25, from <https://link.aps.org/doi/10.1103/PhysRevE.91.041003> doi: 10.1103/PhysRevE.91.041003